



**HAL**  
open science

# Selective identification of cyclopentaring-fused PAHs and side-substituted PAHs in a low pressure premixed sooting flame by photoelectron photoion coincidence spectroscopy

X. Mercier, A. Faccinetto, S. Batut, G. Vanhove, D. Božanić, H. Hróðmarsson, G. Garcia, L. Nahon

## ► To cite this version:

X. Mercier, A. Faccinetto, S. Batut, G. Vanhove, D. Božanić, et al.. Selective identification of cyclopentaring-fused PAHs and side-substituted PAHs in a low pressure premixed sooting flame by photoelectron photoion coincidence spectroscopy. *Physical Chemistry Chemical Physics*, 2020, 22 (28), pp.15926-15944. 10.1039/D0CP02740E . hal-03016086

**HAL Id: hal-03016086**

**<https://hal.science/hal-03016086>**

Submitted on 20 Nov 2020

**HAL** is a multi-disciplinary open access archive for the deposit and dissemination of scientific research documents, whether they are published or not. The documents may come from teaching and research institutions in France or abroad, or from public or private research centers.

L'archive ouverte pluridisciplinaire **HAL**, est destinée au dépôt et à la diffusion de documents scientifiques de niveau recherche, publiés ou non, émanant des établissements d'enseignement et de recherche français ou étrangers, des laboratoires publics ou privés.

1           **Title: Selective identification of cyclopentaring-fused PAHs and side-**  
2           **substituted PAHs in a low pressure premixed sooting flame by photoelectron**  
3                           **photoion coincidence spectroscopy**

4  
5   **Authors:** X. Mercier<sup>1\*</sup>, A. Faccinetto<sup>1</sup>, S. Batut<sup>1</sup>, G. Vanhove<sup>1</sup>, D. K. Bozanic<sup>2†</sup>, H. R.  
6   Hrodmarsson<sup>2,‡</sup>, G. A. Garcia<sup>2</sup>, L. Nahon<sup>2</sup>

7  
8   **Affiliations:**

9   <sup>1</sup>Université Lille, CNRS, UMR 8522 - PC2A - Physicochimie des Processus de Combustion et de l'Atmosphère, F-  
10   59000 Lille, France,

11   <sup>2</sup> Synchrotron SOLEIL, L'Orme des Merisiers, St. Aubin, BP 48, 91192 Gif sur Yvette, France

12  
13   \*Correspondence to: Xavier Mercier ([xavier.mercier@univ-lille.fr](mailto:xavier.mercier@univ-lille.fr)). Tel: + 33 3 20 43 48 04

14   <sup>†</sup>Current institutional address: Vinča Institute of Nuclear Sciences, University of Belgrade, P.O. Box 522, 11001  
15   Belgrade, Serbia

16   <sup>‡</sup>Current institutional address: Laboratory for Astrophysics, Leiden Observatory, Leiden University, PO Box 9513,  
17   NL-2300 RA Leiden, The Netherlands

18  
19   **Abstract:**

20       This work reports on the selective on-line identification of polycyclic aromatic hydrocarbons  
21   (PAHs) formed in a low-pressure methane sooting flame, carried out using the double imaging  
22   Photoelectron Photoion Coincidence Spectroscopy method (*i*<sup>2</sup>PEPICO) on the DESIRS VUV  
23   beamline at the synchrotron SOLEIL. Generally, this work demonstrates the capabilities of the  
24   *i*<sup>2</sup>PEPICO method to identify PAHs in sooting flames, and in particular to distinguish  
25   cyclopentaring-fused PAHs (CP-PAHs) and side-substituted PAHs from their benzenoid  
26   isomers. Experimental threshold photoelectron spectra of four CP-PAHs: acenaphthylene (C<sub>12</sub>H<sub>8</sub>,  
27   152 *m/z*), acenaphthene (C<sub>12</sub>H<sub>10</sub>, 154 *m/z*), fluoranthene (C<sub>16</sub>H<sub>10</sub>, 202 *m/z*) and  
28   benzo(ghi)fluoranthene (C<sub>18</sub>H<sub>10</sub>, 226 *m/z*) are also reported for the first time.

29

30 **Keywords:** threshold photoelectron spectroscopy (TPES), electron/ion coincidence, polycyclic

31 aromatic hydrocarbons (PAHs), soot, nucleation

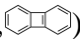
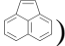
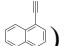
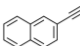
## 32 1. Introduction

33 Soot particles released at the exhaust of combustion processes are subject to special attention  
34 because of their well-documented detrimental impact on the human health and environment.  
35 Soot particles in the atmosphere are at the origin of allergic rhinitis and other affections of the  
36 respiratory system<sup>1</sup>. Many hydrocarbons adsorbed at the surface of soot particles and formed  
37 during the combustion process are known to be toxic and to have mutagenic and/or carcinogenic  
38 health effects<sup>2,3</sup>, and the inhalation of soot particles has been correlated to a wide variety of acute  
39 and chronic diseases<sup>4</sup>. In the environment, especially when released in the high troposphere by  
40 aeronautic jet engines for instance, soot particles impact the radiative forcing of the atmosphere  
41 as they can absorb and scatter the solar radiation (direct effect) or act as cloud/ice condensation  
42 nuclei and trigger the formation of persistent clouds (indirect effect), thereby affecting the local  
43 climate<sup>5,6</sup>. The detailed chemical characterization of soot particles can therefore provide crucial  
44 information to better assess their toxicity and atmospheric reactivity, and furthermore, help to  
45 clarify their formation process, which so far is not completely understood.

46 The formation of soot particles in flames is known to be strongly correlated to reaction  
47 pathways involving polycyclic aromatic hydrocarbons (PAHs), which are considered the main  
48 precursors of soot particles. Although the growth of PAHs is widely accepted to be driven by the  
49 HACA mechanism<sup>7</sup> (Hydrogen Abstraction Acetylene Addition), alternative reaction pathways  
50 have also been suggested<sup>8-13</sup>. In order to evaluate the relative importance of these pathways,  
51 experimental data are needed to, firstly, unambiguously identify the chemical species involved in  
52 the soot formation process, and secondly, to measure their in-flame concentrations. However,  
53 recent atomic force microscopy experiments<sup>14</sup> demonstrated that the growth process of PAHs  
54 naturally results in the formation of a variety of structural isomers that can be found adsorbed on  
55 the soot particles surface. At a given mass, structural isomers of PAHs can be very difficult to  
56 discriminate with traditional analytical techniques as their number rapidly increases with the

57 number of carbon atoms in the molecule<sup>15</sup>. In-situ laser based methods such as laser induced  
58 fluorescence (LIF) can generally provide qualitative data about PAH formation in flames, as well  
59 as the PAH class size and their localization in the flame<sup>16-22</sup>, but such methods are incapable of  
60 unfolding the contributions of individual species. It has been recently shown that better  
61 discrimination can be achieved by using relatively simple spectral models for the interpretation  
62 of the experimental fluorescence spectra that rely on the use of tabulated fluorescence spectra of  
63 individual PAHs<sup>23,24</sup>. Not only these methods allow the identification of the main PAHs formed  
64 in flames, but in particularly favorable cases they can even distinguish between structural  
65 isomers such as pyrene and fluoranthene. However, such approaches do not yet allow  
66 quantitative measurements. The determination of mole fraction profiles of PAHs in flames by  
67 LIF indeed requires ex-situ measurements, such as those provided by complex laboratory setups  
68 like Jet-Cooled Laser Induced Fluorescence (JCLIF)<sup>25,26</sup>. However, JCLIF requires fine  
69 adjustment of the excitation laser wavelength to a resonant transition of a specific target PAH,  
70 which limits the measurement capability to a few PAHs having well-known spectral properties,  
71 and to only one isomeric structure at a time.

72 In comparison, mass spectrometry-based methods based on time-of-flight are multiplex in  
73 mass, and allow the simultaneous measurement of all the molecular species in the sample but can  
74 generally not distinguish structural isomers. In addition, the high ionization energies used in  
75 typical setups based on electron impact lead to complex fragmentation patterns that complicate  
76 the identification of the parent ions. In this context, tunable vacuum ultraviolet (VUV) radiation,  
77 such as the one provided by synchrotron-based techniques, is an attractive way to obtain  
78 selective PAHs concentration profiles in flames because of its ability to distinguish structural  
79 isomers<sup>27-30</sup> via spectral discrimination, and to avoid or limit the amount of fragmentation by  
80 ionizing close to the threshold. Different research groups highlighted the capabilities of such  
81 techniques for the selective and quantitative measurement of species formed in rich flames<sup>31-34</sup>.

82 In the cited works, unknown species are identified through their photoionization efficiency (PIE)  
83 curve, which consists of the integrated ion signal against the photon energy. The first ionization  
84 of PAHs commonly leads to the formation of stable molecular cations that can be detected  
85 independently by mass spectrometry. Therefore, a PIE curve recorded for a specific mass with  
86 tunable Synchrotron Radiation (SR) in the range of, and immediately above the first ionization  
87 energy of PAHs ( $IE = 7-11.5$  eV) in principle allows the identification of structural isomers once  
88 their individual spectral contribution are known<sup>28,31,34-36</sup>. However, these curves integrate over  
89 all available states of the cation at a given photon energy, and therefore lack sufficient spectral  
90 structures to deliver an unambiguous interpretation, especially when several isomers coexist at  
91 the same  $m/z$  and have close  $IE$  values. This is notably the case of  $m/z = 152$ , studied in this  
92 work, which is generally associated to four different main isomers<sup>37</sup> in flame investigations:  
93 biphenylene ( $IE=7.58$  eV, ) , acenaphthylene ( $IE=8.02$  eV, ) , 1-ethynyl-naphthalene  
94 ( $IE=8.11$  eV, ) and 2-ethynyl-naphthalene ( $IE=8.03$  eV, ) . In this case, the distinction  
95 between acenaphthylene and 2-ethynyl-naphthalene based only on their PIE curves is impossible.  
96 We note, however, that in some cases identification can be greatly helped by the appearance of  
97 autoionization features in the PIE curves, such as the ones seen for coronene<sup>38</sup>.

98 As a first approximation, ignoring autoionization resonances, a PIE curve corresponds to the  
99 integral of the photoelectron spectrum (PES) at a given photon energy and therefore contains  
100 much less sharp spectroscopic features, i.e. possesses a much weaker analytical ability in  
101 disentangling structural isomer ions detected at the same  $m/z$ . For this reason, photoelectron-  
102 photoion coincidence spectroscopy (PEPICO) has been demonstrated in the last years to be a  
103 powerful tool for the identification of structural isomers in complex gas-phase environments  
104 such as flames, combustion reactors and oxidation chambers<sup>39-47</sup>. This technique enables the  
105 recording of photoelectron spectra (PES) of the mass-selected ionized detected species. Because  
106 of the richer vibronic structure as compared to PIE curves, the PES acts as a unique fingerprint

107 providing unambiguous information about its structure<sup>43,48</sup>. Such a fine analysis of complex  
108 mixtures via mass-selected PES is based upon the comparison with either known experimental  
109 PES of pure compounds or, alternatively, PES obtained from ab-initio calculations. Notably,  
110 Felsmann et al.<sup>41</sup> demonstrated the capabilities, including the sensitivity, of the double imaging  
111 photoelectron photoion coincidence spectrometer  $i^2$ PEPICO technique for the identification of  
112 different structural isomers formed in dimethyl ether and cyclopentene flames. They identified  
113 for the first time without ambiguity in the low pressure cyclopentene flame, the contributions of  
114 1-penten-3-yne in competition with the much larger signal of 1,3-cyclopentadiene. Different  
115 other aromatic species up to 128  $m/z$  were also detected.

116 The aim of this work is to explore the capabilities of the  $i^2$ PEPICO method for the detection  
117 of PAHs in sooting flames, more specifically focusing on the identification of gas phase PAHs  
118 isomers formed in the nucleation region of a sooting flame. This study has been carried out on  
119 the DESIRS VUV beamline at the SOLEIL synchrotron by using the permanent  $i^2$ PEPICO-based  
120 experimental setup SAPHIRS, which was coupled to a low pressure premixed  $\text{CH}_4/\text{O}_2/\text{N}_2$   
121 sooting flame stabilized at the pressure  $p=26.66$  kPa (200 torr), with an equivalence ratio  $\phi=2.32$ .  
122 This flame was chosen for several reasons. First, it has already been the subject of several studies  
123 by some of the co-authors dedicated to PAHs and soot formation<sup>25,49–54</sup> with a variety of  
124 diagnostics, therefore providing an ideal benchmark case for the present work. Second, this  
125 flame is a lightly sooting flame characterized by a soot volume fraction profile reaching values  
126 of the order of a few ppb in the burnt gases<sup>53</sup>. The study of sooting flames with the  $i^2$ PEPICO  
127 setup introduces an additional difficulty for sampling measurements in comparison to the non-  
128 sooting flames studies reported above. Because of the formation of soot particles, the clogging of  
129 the sampling probe becomes a critical issue during the recording of photoelectron spectra that  
130 can take up to several hours. The choice of this lightly sooting flame was also aimed at limiting  
131 this issue. Note, however, that contrary to PIE curves where the photon energy needs to be

132 scanned and thus a high reactor stability is required, fixed-photon energy photoelectron  
133 spectroscopy can also be recorded with the  $i^2$ PEPICO setup. This approach can be much faster  
134 and overcomes the need for stability, albeit at the expense of energy resolution, as discussed  
135 further in the text and demonstrated in the context of flames<sup>41,43</sup>.

136 To demonstrate the capability of the  $i^2$ PEPICO setup for PAH measurements and isomer  
137 discrimination in sooting flames, we specifically focused on the nucleation region of the flame,  
138 i.e. the zone where the first nascent soot particles (NSPs) are formed. One specific outcome of  
139 this work was to clearly highlight the formation of cyclopentaring-fused-PAHs (CP-PAHs)  
140 whose structure contains five-membered carbon rings, which have already been proposed in the  
141 literature to be important intermediates on the formation of NSPs<sup>11,12,55-58</sup>. CP-PAHs often share  
142 the same molecular formula as six-membered ring PAHs, and are thus impossible to distinguish  
143 with common mass spectrometry setups. Moreover, we were also interested in revealing the  
144 presence, or absence, of side-substituted PAHs in the sampled gases. The  $i^2$ PEPICO setup  
145 provides a unique possibility to record the PES for each of the peaks on the mass spectra  
146 simultaneously, allowing the identification of the formed PAHs via their electronic fingerprints,  
147 provided that individual PES of the detected species are known. PES of small hydrocarbons are  
148 globally well documented in the literature, which makes their identification straightforward.  
149 However, the number of isomers quickly increases with the size of the molecule making the  
150 identification of larger molecules, such as PAHs more complex. In particular, the selective  
151 identification of some of these PAH isomers required the measurement of the PES of several  
152 pure CP-PAHs which not available in the literature at the time of our experiments. Hence, the  
153 PES of fluoranthene ( $C_{16}H_{10}$ , 202  $m/z$ ), acenaphthylene ( $C_{12}H_8$ , 152  $m/z$ ), acenaphthene ( $C_{12}H_{10}$ ,  
154 154  $m/z$ ) and benzo(ghi)fluoranthene ( $C_{18}H_{10}$ , 226  $m/z$ ) are also reported for the first time in this  
155 paper.



156 The experimental setup we used can be operated in two modes: (1) the threshold-PES mode  
157 enabling the determination of the PES by scanning the photon energy while selecting only quasi-  
158 zero kinetic energy electron and (2) the PES mode in which the full PES is encoded into a single  
159 electron image recorded at fixed photon energy. In both modes all the masses are acquired  
160 simultaneously, providing mass-selected TPES and PES data. A comparison between the results  
161 obtained with these two different modes of operation is also reported in this paper. Benefits,  
162 capabilities and limitations of both modes for PAHs, side-substituted PAHs and CP-PAHs  
163 identification are then discussed.

164

## 165 2. Experimental Setup

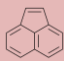
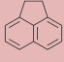
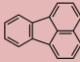

### 166 2.1 Experimental setup used for the determination of PES and PIE curves of 167 acenaphthene, acenaphthylene, fluoranthene and benzo(ghi)fluoranthene

168

169 In order to enable the analysis of specific detected masses and especially highlight the  
170 presence of some CP-PAHs, the measurement of PES and PIE curves of four CP-PAHs currently  
171 missing in the literature and likely formed in sooting flames has been carried out in this work.  
172 These species of interest were acenaphthylene ( $C_{12}H_8$ , 152  $m/z$ ), acenaphthene ( $C_{12}H_{10}$ , 154  $m/z$ ),  
173 fluoranthene ( $C_{12}H_{10}$ , 202  $m/z$ ) and benzo(ghi)fluoranthene ( $C_{18}H_{10}$ , 226  $m/z$ ).

174 The spectra of these species have been recorded by depositing the pure CP-PAHs (98-99%  
175 purity, Aldrich) in an in-vacuum stainless-steel oven. **The experimental device has been already**  
176 **described in detail in a previous work<sup>59</sup>.** He (0.5 bar) was flowed across the oven to carry the  
177 PAH vapor before expansion through a 70  $\mu\text{m}$  nozzle to form a molecular beam which crossed  
178 the two consecutive skimmers of the multipurpose SAPHIRS chamber<sup>60</sup> before reaching the  
179 ionization region. The temperature of the oven has been adjusted according to each CP-PAHs to  
180 generate a vapor pressure enabling the recording of PES with Signal-To-Noise ratio  $\text{SNR} > 3$ .

181 **Table 1** shows the working temperatures and consumption of the four compounds studied in this  
 182 work. The temperatures of the nozzle and oven were optimized to get around 6000 events/second  
 183 at the highest scan energy, which resulted in high quality scans with minimal consumption.  
 184

m/z	Molecular formula	Compound	Structure	Temperature of oven / nozzle (°C)	Total consumption (mg)
152	C <sub>12</sub> H <sub>8</sub>	Acenaphthylene		53/63	60
154	C <sub>12</sub> H <sub>10</sub>	Acenaphthene		55/65	50
202	C <sub>16</sub> H <sub>10</sub>	Fluoranthene		120/130	1215
226	C <sub>18</sub> H <sub>10</sub>	Benzo(ghi)fluoranthene		120/135	12

185

186 *Table 1: Experimental conditions for PES and PIE curves measurements*

187

188 The undulator-based DESIRS beamline<sup>61</sup> was set to provide  $\sim 5 \times 10^{12}$  photons/sec with a  
 189 spectral bandwidth of 10 meV at 10 eV. A pressure of 0.14 mbar of Kr filled the gas filter to  
 190 ensure spectral purity in our energy range<sup>62</sup> by suppressing the high harmonics of the undulator.  
 191 The energy scales were absolutely calibrated using either the 4p<sup>5</sup> 5s(3/2) Kr absorption line<sup>63</sup>  
 192 from the gas filter, as visible in the total ion yields, or the third-order ionization energy of He as  
 193 reported in the NIST database. The energy scan data have been normalized by the photon flux  
 194 measured with an AXUV100 photodiode from International Radiation Detectors, Inc.

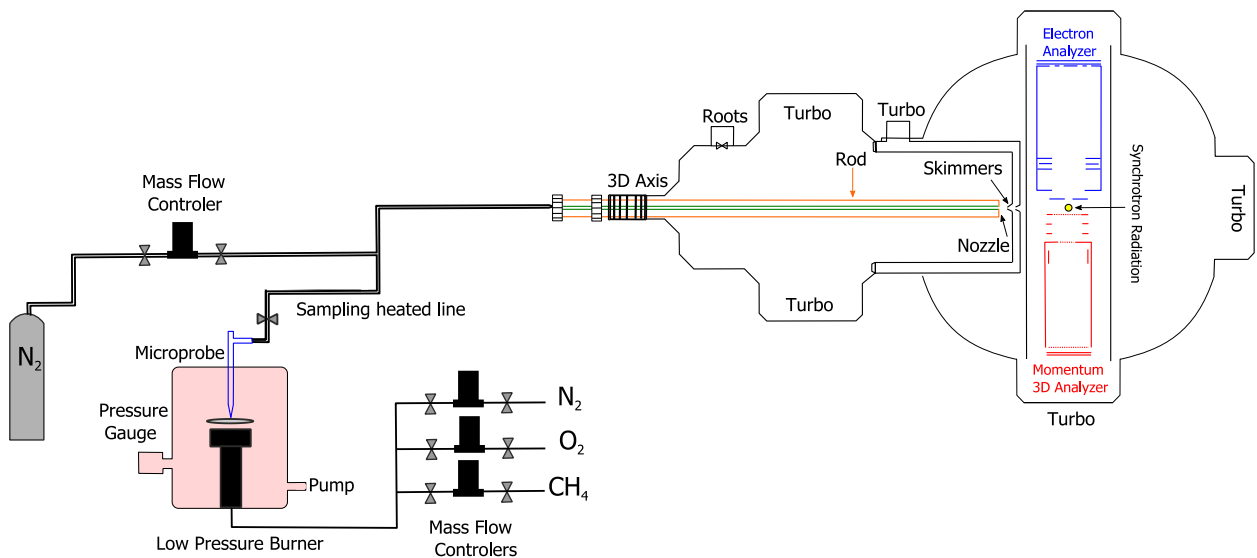
195 The DELICIOUS3 i<sup>2</sup>PEPICO spectrometer<sup>64</sup>, which couples a VMI spectrometer on the  
 196 electron side and a 3D-momentum imager spectrometer on the ion side, was used in the  
 197 coincidence mode to obtain the photoelectron images correlated to a given ion mass and position  
 198 at each scan point (or fixed photon energy), with a continuous extraction field of 88 V/cm. Note  
 199 that the selection of a given ion arrival position in the detector (ion Region Of Interest, or ion  
 200 ROI) ensures that only molecules originated in the flame or from HAP vaporization, and thus

201 having a net velocity along the molecular beam, are considered, decreasing the background  
 202 signal coming from the  $10^{-7}$  mbar base pressure of the ionization chamber<sup>65</sup>. TPES were obtained  
 203 with the Slow Photoelectron Spectroscopy method described previously<sup>66</sup>. For the standards  
 204 mentioned in *Table 1*, photoelectrons from 0 to 70 meV were used to build the TPES, which  
 205 provided an electron kinetic energy resolution of 10 meV as measured on the third-order  
 206 ionization of He, leading to an overall resolution of 14 meV and an overall absolute accuracy for  
 207 the *IE* determination of 0.003 eV.

208

## 209 2.2 Flame sampling experiment

210 A schematic representation of the experimental setup used for this work is reported in *fig. 1*.



211

212

*Figure 1: Experimental Setup*

213

214 As mentioned in the introduction, we investigated a low pressure premixed sooting flame of  
 215 methane/oxygen/nitrogen characterized by a fuel-to-oxidizer equivalence ratio  $\phi = 2.32$ . The  
 216 pressure inside the vessel was controlled and kept constant at 26.66 kPa (200 torr) thanks to an  
 217 automatic pressure regulation valve. More details about this flame and the low pressure vessel  
 218 arrangement can be found in previous publications<sup>25,26</sup>. The experimental flame conditions are  
 219 reported in *Table 2*.

$\phi$	C/O	$x_{CH_4}$	$x_{O_2}$	$x_{N_2}$
2.32	0.58	0.462	0.398	0.14

*Table 2: Composition of the studied flame. The total flow rate was 3.96 L/min STP.*

During the flame experiments, species were continuously extracted from the flame through a thin microprobe having a 300  $\mu\text{m}$  aperture diameter. The pressure inside the line was kept constant to  $10 \pm 0.01$  mbar. The whole transfer line from the microprobe down to the skimmer located in the SAPHIRS chamber was heated up to 140  $^\circ\text{C}$  to limit the condensation of the PAHs as discussed in a previous work<sup>67</sup>. Extracted species were directly expanded in the SAPHIRS chamber through a nozzle with an orifice aperture of 500  $\mu\text{m}$ . This relatively large orifice was used to optimize the SNR and the sensitivity of the measurement at the cost of a less efficiently cooled and collimated supersonic beam. The supersonic beam was then double skimmed before finally crossing the synchrotron beam at a right angle in the ion source of the i<sup>2</sup>PEPICO spectrometer. The position of the nozzle with respect to the ionization beam was aligned and optimized by using a dedicated N<sub>2</sub> line.

With this setup, we implicitly made the choice to limit the detection to stable species only. Indeed, the use of a microprobe, instead of a sampling cone and skimmer device as usually implemented for generating a molecular beam, does not allow the capture of radicals. In return, this system offers a much lower detection limit than typical molecular beam mass spectrometry setups. We estimated our detection limit in the order of 0.1 ppm, i.e. at least one order of magnitude lower than the typical sensitivity of 1-10 ppm of molecular beam mass spectrometry setups reported in the literature<sup>31,32,68,69</sup>. This value was estimated from the comparison with quantitative measurements carried out by JCLIF in the same flame<sup>25</sup> reporting peak mole fractions of pyrene and fluoranthene around 0.4 and 0.1 ppm.

243 In this work, we carried out either the recording of ion mass- and ROI-selected PES data at  
244 fixed photon energy (denoted as PES spectra in figures) and/or TPES spectra by scanning the  
245 photon energy<sup>66</sup>. PES typically required around 30 minutes of data acquisition to get a  
246 satisfactory SNR (typically SNR>3). The TPES mode greatly improves the spectral resolution  
247 but requires an acquisition of a few hours because the photon energy needs to be scanned. For  
248 the flame experiments, the photoelectron window used to obtain the TPES was increased to 200  
249 meV to achieve a better SNR, leading to an overall energy resolution of 35 meV.

250 Most PES experiments were performed at 8 eV to favor the ionization of small PAHs and  
251 limit fragmentation of the parent cations. However, we also report a few spectra recorded at  
252 higher *IE* up to 9-10 eV, in order to broaden the range of detected species towards small  
253 aromatic and aliphatic compounds.

254 As mentioned above, we focused our measurements on the beginning of the soot nucleation  
255 zone of the flame as determined in previous work<sup>25,54</sup>, which corresponds to a region located  
256 from height above the burner (HAB) 9 to 15 mm where the temperature of the flame has been  
257 determined be nearly constant around 1760±20 K<sup>52</sup>. Note that around 80 different peaks in the  
258 40-252 *m/z* range have been detected in this zone.

259

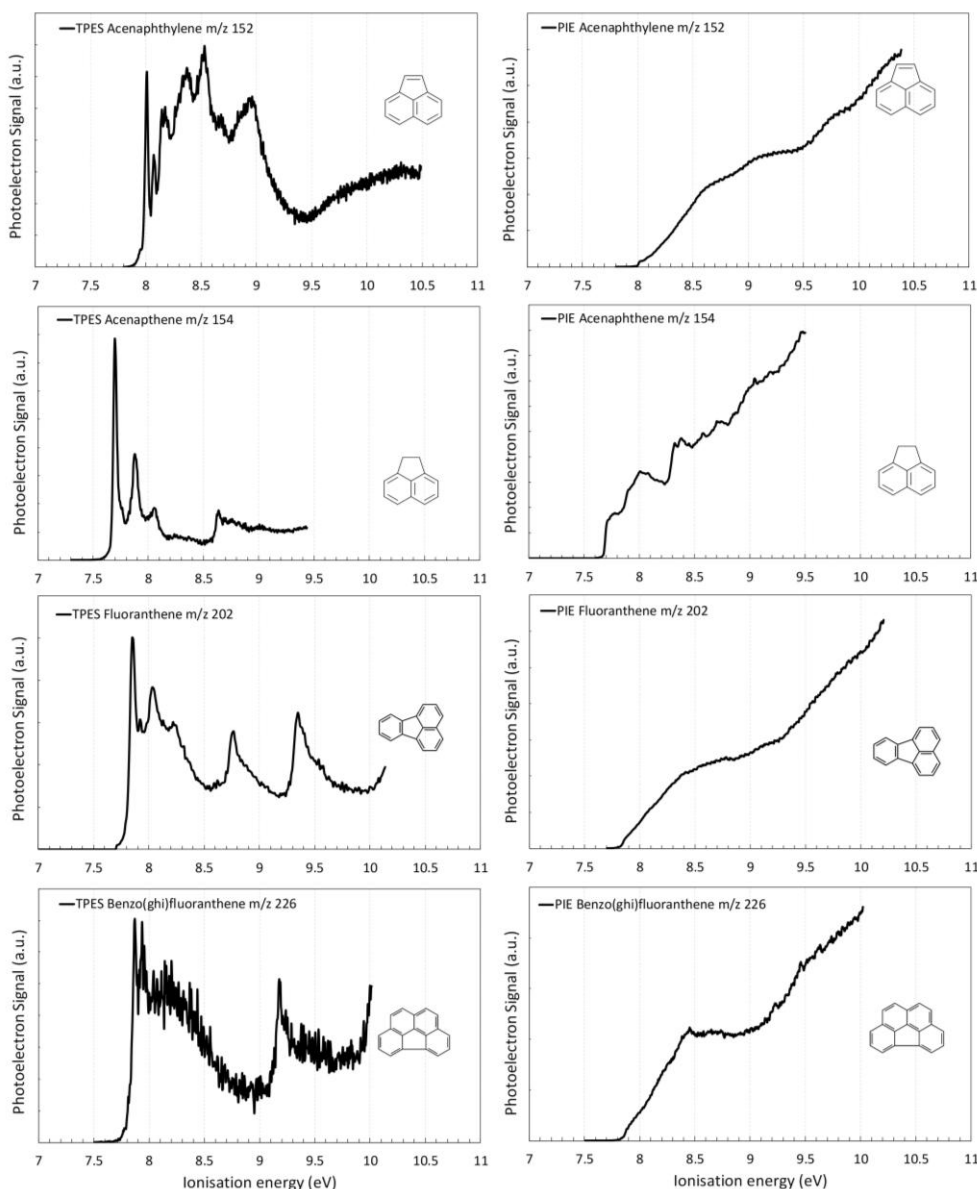
### 260 3. Results and discussion

261

#### 262 3.1 Measurements of the reference PES and PIE curves of acenaphthene, 263 acenaphthylene, fluoranthene and benzo(ghi)fluoranthene

264 The TPES and PIE curves recorded for the four CP-PAHs are shown in *fig.2*. Note that all the  
265 data shown correspond to the parent ion selection. No fragmentation channels have been  
266 identified in the TOF mass spectra for any of the four PAHs considered here, up to 10.5 eV.  
267 While *IE* values have already been published in the literature for acenaphthene, acenaphthylene

268 and fluoranthene<sup>37</sup>, the hereby reported TPES for these species correspond to new and unique  
269 reference spectra to the best of our knowledge. Concerning benzo(ghi)fluoranthene, neither *IE*  
270 values nor PES or PIE curves were available in the literature. Note that the SNR is inferior in this  
271 last spectrum than in the other ones due to the much lower vapor pressure of  
272 benzo(ghi)fluoranthene. However, the recorded spectrum still highlights clearly distinguishable  
273 and characteristic vibronic structures. Such spectra are likely to be used for the identification of  
274 these species in various applications including combustion but also other scientific fields like  
275 astrophysics. The unique character of these new data remains therefore of significant interest  
276 beyond the scope of combustion studies. Notably, the spectrum of fluoranthene, which is a  
277 structural isomer of pyrene, potentially remains of great interest for both these communities  
278 considering the importance of pyrene in rich flame chemistry and interstellar medium. Although  
279 pyrene itself has not yet been discovered in any interstellar media, PAHs and PAH cations  
280 remain very astrophysically relevant. Kim et al.<sup>70</sup> reported that the infrared spectrum of the  
281 pyrene cation very closely resembles the interstellar unidentified infrared emission bands.  
282 Furthermore, this work also opens a new way to individually identify these PAHs in interstellar  
283 ice analogs and carbonaceous chondrites<sup>71,72</sup>.  
284



285

286

**Figure 2:** TPES (left column) and PIE curves (right column) of the four studied PAHs

287

288

289

290

291

292

293

294

The four measured TPES show strong distinguishable spectral features from which it is possible to extract the corresponding adiabatic ionization energy ( $IE_{ad}$ ).  $IE_{ad}$  values are important as they are widely used to identify structural isomers in VUV-photoionization mass spectrometry experiments. In this work, the experimental  $IE_{ad}$  have been measured by fitting a Gaussian peak to the first transition of each spectrum, which is also the most intense band, meaning that there is little geometric change of the molecular structure upon ionization (favorable FC factors), which is typical of PAHs<sup>38,73,74</sup>. The determined values, from the maximum of the Gaussian fitting

295 function, are reported in the first column of *table 3* and compared to measured values provided  
 296 by the literature and referenced in the NIST Webbook. Note that for the three components for  
 297 which  $IE_{ad}$  was previously known, our data provides an increased accuracy on the values.  
 298

m/z	Molecular formula	Compound	$IE_{ad}$ (eV)					
			This work			Literature		
152	C <sub>12</sub> H <sub>8</sub>	Acenaphthylene	8.012±0.003	8.02±0.04 <sup>a</sup>	8.22±0.01 <sup>b</sup>			
154	C <sub>12</sub> H <sub>10</sub>	Acenaphthene	7.700±0.003	7.68±0.05 <sup>c</sup>	7.73±0.01 <sup>b</sup>	7.66 <sup>d</sup>	7.76±0.03 <sup>e</sup>	7.82±0.04 <sup>a</sup>
202	C <sub>16</sub> H <sub>10</sub>	Fluoranthene	7.860±0.003	7.90±0.1 <sup>f</sup>	7.95±0.04 <sup>a</sup>	7.80±0.01 <sup>b</sup>	7.72 <sup>g</sup>	
226	C <sub>18</sub> H <sub>10</sub>	Benzo(ghi)fluoranthene	7.874±0.003					

299

300 *Table 3: Determined first adiabatic ionization energy compared to referenced values<sup>37</sup>*

301 <sup>a</sup>Boschi et al.<sup>75</sup>, <sup>b</sup>Dewar et al.<sup>76</sup>, <sup>c</sup>Mautner et al.<sup>77</sup>, <sup>d</sup>Kinoshita et al.<sup>78</sup>,

302 <sup>e</sup>Heilbronner et al.<sup>79</sup>, <sup>f</sup>Ling and Lifshitz<sup>80</sup>, <sup>g</sup>Slifkin and Allison<sup>81</sup>

303

304 As can be seen in *table 3*, although for the most part our data agree with the literature values  
 305 within the uncertainty, differences in  $IE_{ad}$  of more than 100 meV can be observed, which show  
 306 potential deficiencies in the existing databases and the need of upgrading these values to meet  
 307 the requirements of modern analytical experiments, especially in the context of species  
 308 identification in complex mixtures.

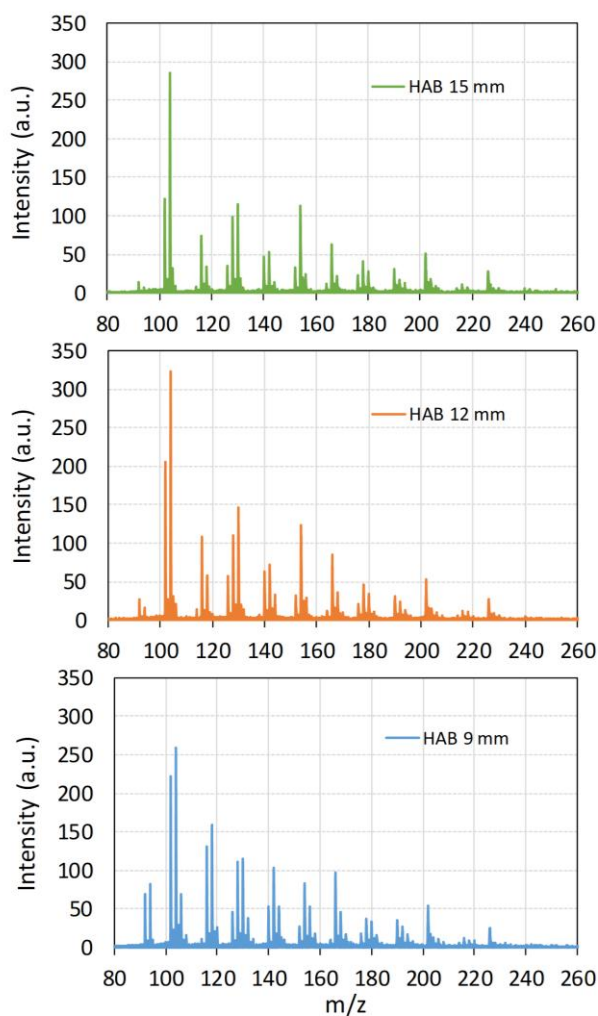
309 Beyond the  $IE$  values, the overall shape of the TPES is relevant for the analysis of combustion  
 310 processes, especially for the ground electronic state (typically over the first 1-1.5 eV above  $IE_{ad}$ ).  
 311 Without entering into a detailed analysis, which is beyond the scope of this work, the FC  
 312 envelope of the ground electronic state of the four species shows quite a rich vibrational structure  
 313 which is a molecular fingerprint for the analysis of complex mixtures. As discussed above, TPES



314 fingerprints are much sharper and molecule-specific than the PIE step functions (especially for  
315 acenaphthylene and fluoranthene) and are therefore more appropriate as reference functions for  
316 fitting the experimental data obtained from the analysis of complex mixtures.

### 317 318 **3.2 Implementation of the $i^2$ PEPICO setup for the identification of PAHs formed in** 319 **flames**

320 *Figure 3* shows a zoom of the mass spectra recorded at a fixed photon energy of 8 eV and for  
321 three distinct sampling HABs (9, 12 and 15 mm above the burner) corresponding to the  
322 nucleation zone of the flame. Around 80 different peaks, ranging from 40 to 252  $m/z$ , have been  
323 detected.



324

325

*Figure 3: Zoom of the mass spectrum of the flame acquired at photon energy 8 eV*

326 *for different heights above the burner.*

327 Some peaks consistent to CP-PAHs and side-substituted PAHs can be noted in *fig. 3* at 152  
328  $m/z$  ( $C_{12}H_8$ ), 154  $m/z$  ( $C_{12}H_{10}$ ), 166  $m/z$  ( $C_{13}H_{10}$ ), 190  $m/z$  ( $C_{15}H_{10}$ ), 202  $m/z$  ( $C_{16}H_{10}$ ), 216  $m/z$   
329 ( $C_{17}H_{12}$ ), 226  $m/z$  ( $C_{18}H_{10}$ ), and 252  $m/z$  ( $C_{20}H_{12}$ ). As mentioned above, the exhaustive analysis  
330 of all detected masses is beyond the scope of this work, and here we focus on those for which  
331 this study can offer the most interesting methodological and mechanistical information, as  
332 discussed below.

333 To this end, the **remaining** of this section is organized in two main parts. The first one is  
334 dedicated to the implementation of the  $i^2$ PEPICO setup for the identification of small aromatic  
335 species well known to be formed in sooting flames. The objective of this first part is to check the  
336 performance of the  $i^2$ PEPICO apparatus for this relatively new task in the context of sooting  
337 flames studies. In the second part, we focus on the study of four different detected masses in our  
338 flame, expected to correspond to moderate-sized PAHs that are very likely involved in the soot  
339 formation mechanisms. These species correspond to 152  $m/z$  ( $C_{12}H_8$ ), 154  $m/z$  ( $C_{12}H_{10}$ ), 202  $m/z$   
340 ( $C_{16}H_{10}$ ) and 226  $m/z$  ( $C_{18}H_{10}$ ).

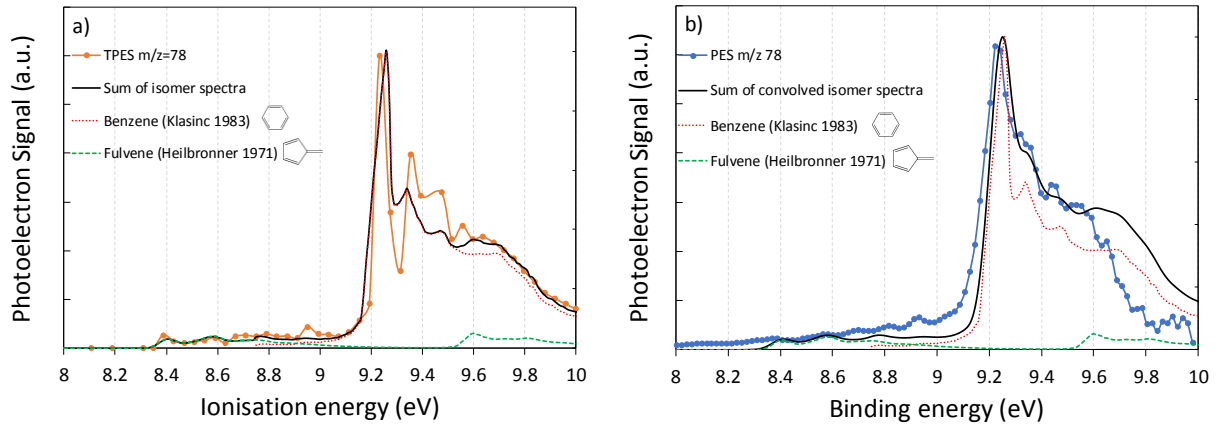
341 The identification method we used relies on the analysis of spectral structures of the  
342 experimental TPES measured at different HAB in the nucleation region of the flame. The  
343 identification of the species corresponding to the measured spectral structure is carried out by  
344 comparing reference PES of individual PAHs (provided by the literature or from this work) with  
345 the one acquired in the flame experiments. **To perform these comparisons, it has been necessary**  
346 **to adjust the spectral resolution of the reference spectra when they were recorded with a better**  
347 **spectral resolution than the experimental spectra. This has been carried out by convolving the**  
348 **reference spectra provided by the literature to a Gaussian function to enlarge the spectral**  
349 **structures of these spectra. The shape of the Gaussian function has been systematically adjusted**  
350 **according to the resolution of the reference spectra, which came from different sources, in order**  
351 **to get the best match with our experimental spectral structures.**

352 **3.2.1 Analysis of the species at 78  $m/z$  ( $C_6H_6$ )**

353 Benzene is a species of great interest for soot formation as it plays a major role in the  
354 initiation of the HACA mechanism. However, benzene is not the only isomer possibly detected  
355 in sooting flames at 78  $m/z$ . Fulvene, which has already been observed in rich flames<sup>82</sup>, is  
356 another likely candidate that has been taken into account to analyze this spectrum. The measured  
357 TPES and PES corresponding to 78  $m/z$  are reported in **fig. 4a and 4b**. The simulated spectrum  
358 (black line), calculated on the basis of the reference spectra of benzene<sup>83</sup> (grey dotted line) and  
359 fulvene<sup>84</sup> (grey dashed line), is also reported on these figures. Due to the poorer spectral  
360 resolution of the PES in comparison with the TPES, we intentionally degraded the simulated  
361 spectrum reported in **fig.4b** using the procedure described by Felsmann et al.<sup>41</sup> for previous  
362 comparable analyses. The PES has been measured with the sampling probe in the sooting flame  
363 positioned at HAB = 12 mm, at a fixed photon energy of 10 eV. This is the reason why the PES  
364 appears truncated, reaching a zero value at 10 eV.

365 The acquisition time for this PES was approximately 30 minutes. The TPES reported in **fig.4a**  
366 required the fine scanning of the ionization energy from 7.2 to 10 eV with a step of 0.04 eV. This  
367 relatively large step has been chosen to limit the acquisition time to 6 hours. Both TPES and PES  
368 clearly show an intense peak at 9.23 eV, in excellent agreement with the *IE* value of 9.24 eV of  
369 the 0-0 vibrational transition of benzene reported in the literature<sup>85</sup>, followed by a series of less  
370 intense vibrational progressions. Also visible in these spectra, especially the TPES, is a series of  
371 weak spectral features between 8.3 and 9.0 eV before the occurrence of the first benzene peak.  
372 This structure is in good agreement with the vibrational structure of the electronic ground state of  
373 fulvene characterized by two main peaks at 8.36 eV and 8.52 eV<sup>85</sup>. The best adjustment we  
374 found between the experimental spectrum (orange line) and the simulated one (black lines) in  
375 **fig.4** has been obtained for relative contributions of benzene and fulvene of 90% and 10%,  
376 respectively. This analysis therefore provides clear evidence of the formation of benzene in the

377 nucleation zone of the flame, in competition with fulvene with a much lower apparent signal  
 378 ratio. This information is however less explicit in the PES reported in *fig.4b* due to the choice of  
 379 the ionization energy which truncates the higher binding energy part of the spectrum.



380  
 381 **Figure 4: TPES and PES (recorded at 10 eV) of 78 m/z at HAB=12 mm.**

382 **Comparison with a simulated spectrum (in black) corresponding to the sum of reference PES of benzene and**  
 383 **fulvene for a signal ratio of 90:10.**

384  
 385 It is to be noted that, in a previous study, the mole fraction of benzene was determined around  
 386 85 ppm at this HAB in this flame by JCLIF<sup>26</sup>. Based on this experimental value, the  
 387 concentration of fulvene can be determined from the relative intensities of the two spectra and  
 388 the knowledge of the ionization cross section at 10 eV. Hence the mole fraction of fulvene  $X_f$   
 389 can be related to the benzene mole fraction  $X_b$  according to the formula:

$$390 \quad X_f = X_b \frac{\sigma_{ib} S_f}{\sigma_{if} S_b} \quad \text{Eq.1}$$

391 where  $\sigma_{ib}$  and  $\sigma_{if}$  correspond to the benzene and fulvene ionization cross sections at 10 eV and  
 392  $S_f/S_b$  corresponds to the relative signal ratio of the contributions of fulvene and benzene. The  
 393 absolute cross-section of benzene at 10 eV has been measured at 25 Mb<sup>86,87</sup>, while for the  
 394 fulvene only an estimated value of 35 Mb is found in the literature<sup>88</sup>. These values lead to an  
 395 estimated mole fraction of fulvene around 7 ppm at 12 mm HAB.

396 Note that the PES, which requires 12 times less time than the recording of the TPES scan, still  
397 provides an adequate resolution and sensitivity for the detection of benzene in these conditions,  
398 with the added advantages of not needing a stable sample, or tunable light, as discussed by  
399 Krüger *et al.*<sup>43</sup> However, the degraded spectral resolution renders the identification of fulvene  
400 somewhat less certain.

401

### 402 **3.2.2 Analysis of the species at 116 $m/z$ ( $C_9H_8$ )**

403 This peak, commonly detected in sooting flames, potentially corresponds to indene, i.e. the  
404 lightest CP-PAHs consisting of one six-member and one five-member ring. The identification of  
405 this species by mass spectrometry methods is not trivial because of the several isomers  
406 coexisting at this  $m/z$ , the most important of which being 1-propynylbenzene and the three  
407 ethynyl-methyl-benzenes<sup>31,41</sup>. *IEs* of 8.14 eV<sup>76</sup> and 8.41 eV<sup>89</sup> have been reported for indene and  
408 1-propynylbenzene respectively, while the *IE* values of 1-ethynyl-4-methylbenzene, 1-ethynyl-3-  
409 methylbenzene and 1-ethynyl-2-methylbenzene are 8.48, 8.63 and 8.61 eV<sup>89</sup>. We show in **fig. 5a**  
410 **and 5b** the comparison of experimental TPES and PES obtained at HAB = 15 mm with reference  
411 spectra for pure indene and 1-propynylbenzene<sup>90</sup>. As in the case of benzene detection, the TPES  
412 in **fig. 5a** required a 6 hours long scan while the PES reported in **fig. 5b** has been recorded with a  
413 much shorter acquisition time of approximately 30 minutes. The spectral resolution of both  
414 reference spectra has been adjusted in order to match our experimental conditions. This has been  
415 done by convolving the reference spectra with a Gaussian function according to the protocol  
416 previously described in Felsmann *et al.*<sup>41</sup>

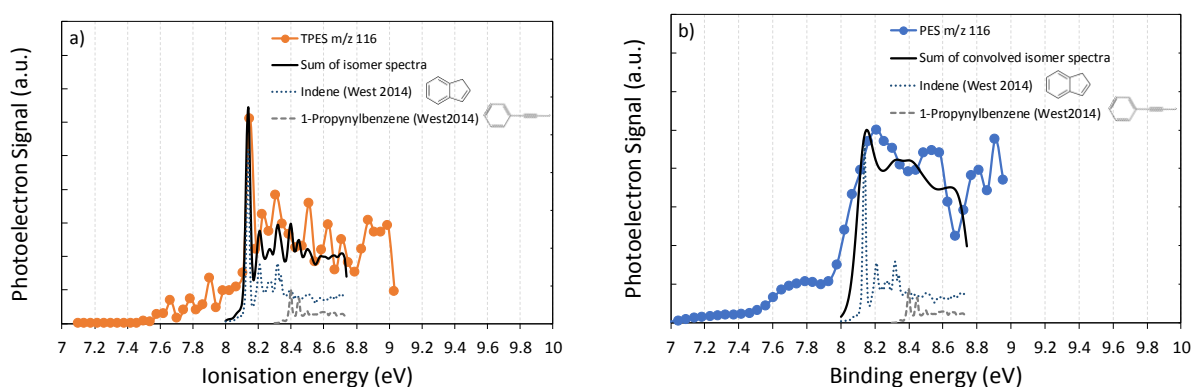
417 Although the TPES of indene reported in **fig. 5a** seems in itself able to explain our spectrum,  
418 we also considered the potential contribution of the only other isomer for which the TPES has  
419 been reported, 1-propynylbenzene. The indene and 1-propynylbenzene contributions associated  
420 to the simulated spectra have been found to be 83% and 17%, respectively. However, it is

421 possible that minor contributions of other structural isomers are present on this spectrum. We  
422 notably observe a slight increase in signal around 8.5 eV which might highlight the presence of  
423 1-ethynyl-4-methylbenzene, a species for which no reference spectrum is currently available.  
424 Moreover, no correspondence could be found either for the small spectral features between 7.6  
425 and 8.0 eV, the lowest IE reported in the literature for 116  $m/z$  being the one of indene<sup>91</sup>.

426

427

428



429

430

**Figure 5: TPES (recorded at 10 eV) and PES of 116  $m/z$  at HAB = 15 mm.**

431 **Comparison with a simulated spectrum (in black) corresponding to the sum of reference PES of indene and 1-**  
432 **propynylbenzene for a signal ratio of 83:17.**

433

434 Our experimental PES in **fig. 5b** shows a very similar structure to the one reported by  
435 Felsmann et al.<sup>41</sup>. In this previous work, the 116  $m/z$  signal was also studied with the same setup  
436 at SOLEIL, but in a low-pressure, rich flame of cyclopentene ( $\phi=1.70$ ,  $p=33.3$  mbar) and using a  
437 molecular beam mass spectrometry configuration for the sampling of the species. The PES  
438 structure highlights a strong feature in excellent agreement with the  $IE_{ad}$  value of 8.14 eV of  
439 indene<sup>76</sup>, which allows its clear identification from this spectrum. Concerning  
440 1-propynylbenzene, its lower concentration in comparison with indene combined with the low  
441 spectral resolution of the PES make its identification less evident from this spectrum. It is

442 interesting to note that the analysis of this mass is in good agreement with previous similar  
443 experiments<sup>41</sup>.

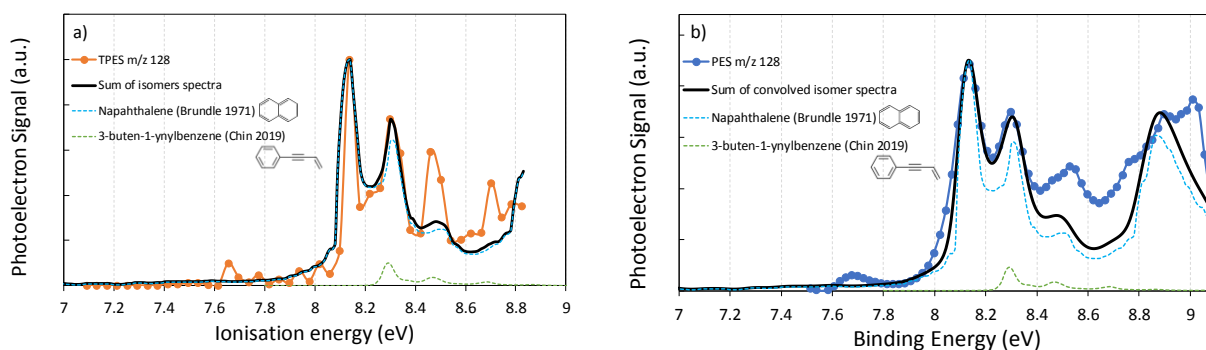
444 Finally, the experimental TPES reported in *fig.5a* shows a much better spectral resolution and  
445 agreement with the sum of indene and 1-propynylbenzene spectra. As for the case of 78 *m/z*, we  
446 however note some slight differences in this PES/TPES comparison which can mainly be  
447 attributed to the degraded SNR of our experiment because of the relatively weak concentration  
448 of these species. The mole fraction of indene has been estimated by modeling to be around  
449 0.5 ppm in the flame<sup>52</sup>. Hence, we can state that the TPES allows an accurate identification of  
450 indene in this flame while the identification of the signal around 8.40-8.50 eV to 1-  
451 propynylbenzene still needs confirmation.

452

### 453 3.2.3 Analysis of the species at 128 *m/z* ( $C_{10}H_8$ )

454 TPES and PES measured at HAB = 15 mm and corresponding to 128 *m/z* are reported in *fig.*  
455 *6*. The PES in *fig. 6b* has been recorded at 10 eV with an acquisition time of 52 minutes, while  
456 the TPES in *fig. 6a* required an acquisition time of 4 hours for scanning the ionization energy  
457 from 7.1 to 9 eV with 0.04 eV steps.

458



459

460 **Figure 6: TPES and PES of 128 *m/z* at HAB=15 mm.**

461 **Comparison with a simulated spectrum (in black) corresponding to the sum of reference PES of naphthalene and**  
462 **3-buten-1-ynyl benzene for a signal ratio of 100:10.**

463

464 The TPES shows an intense peak, which is in perfect agreement with the value of the first *IE*  
465 potential of naphthalene of 8.14 eV<sup>37</sup>. Moreover, the experimental spectrum also features a  
466 vibrational structure characterized by two other weaker spectral bands peaking around 8.30 and  
467 8.50 eV, also in good agreement with the naphthalene reference spectrum<sup>92</sup>. The PES in *fig. 6b*  
468 also provides an adequate resolution for the identification of naphthalene sampled from the  
469 flame. The first three peaks of the vibrational structure of naphthalene are clearly visible in the  
470 PES as well (*fig. 6b*). In addition, the spectrum shows a strong band at 8.85 eV which is also  
471 indicative of naphthalene. It should be noted that we again intentionally degraded the resolution  
472 of the reference spectrum to match the experimental condition of the PES.

473 In both PES and TPES, two spectral regions of the experimental spectra do not match the  
474 reference naphthalene spectrum. The first spectral region is characterized by a weak spectral  
475 feature peaking around 7.65 eV for which we could not find any potential candidate with such a  
476 low *IE* value. Only azulene, with a first *IE*<sub>ad</sub> around 7.42 eV, might be responsible for these  
477 structures<sup>93</sup>, but neither its *IE*<sub>ad</sub> nor its vibronic structure match our spectrum, so that this species  
478 can safely be excluded from the list of potential candidates.

479 The second spectral region not perfectly reproduced by the reference spectrum of naphthalene  
480 is between 8.4 and 8.7 eV. This part of the spectrum notably displays a significant peak around  
481 8.5 eV, which potentially originates from another isomer. Again, we could not find any  
482 compound matching this *IE* value. Chin et al.<sup>94</sup> recently reported simulated PES of some  
483 naphthalene isomers from their Franck–Condon calculations. The spectrum reported in green  
484 dashed lines in *fig.6* corresponds to the calculated spectrum for 3-buten-1-ynyl benzene. This  
485 minor contribution (10% of the naphthalene contribution) improves the fit of the experimental  
486 spectra, but is not sufficient to completely explain the shape of the spectrum around 8.5 eV. A  
487 shift of the 3-buten-1-ynyl benzene calculated spectrum by a few 100 meV's would improve the  
488 correlation with 8.5 eV measured feature in both the PES and TPES.



489 This comparison clearly confirms naphthalene as the main compound at 128  $m/z$ , the mole  
490 fraction of which having been previously measured by JCLIF around 1-2 ppm in this region of  
491 the flame<sup>67</sup>. The uncertainty on the identification of the potential other minor species highlights  
492 the need for reference PES to facilitate the analysis of PAHs formed in sooting flames.

493 To conclude on these first measurements, we can state that the spectral resolution, selectivity  
494 and sensitivity of the  $i^2$ PEPICO apparatus enable the selective detection of PAHs structural  
495 isomers. The TPES, while requiring longer acquisition times provided a more accurate  
496 distinction between structural isomers when reference spectra are available, whereas the faster  
497 recorded PES lead to a degraded spectral resolution and lower SNR in comparison with TPES  
498 experiments. This can limit their usability for the determination of the contributions of minor  
499 species, although they still provide richer information than PIE curves.

500 In the following sections, peaks for larger detected  $m/z$  are investigated. The objective of this  
501 further work is to reveal the potential formation of CP-PAHs and side-substituted PAHs, likely  
502 involved in soot formation, besides the more commonly investigated benzenoid PAHs in the  
503 detected species sampled from the nucleation zone of the flame.

504

### 505 **3.3 Identification of CP-PAHs and side-substituted PAHs in sooting flames**

506 To highlight the capabilities of the  $i^2$ PEPICO method for the identification of PAH isomers,  
507 further work focused on four detected species usually observed in sooting flames for which  
508 structural isomers potentially involving CP-PAHs and side-substituted PAHs might be formed.  
509 In the following, we systematically report the TPES recorded at the very beginning of the soot  
510 inception zone (HAB = 9 mm), and well inside the flame soot nucleation region (HAB = 15  
511 mm). The corresponding spectra have been determined with different energy steps (0.01 eV at  
512 HAB = 9 mm and 0.04 eV at HAB = 15 mm, requiring 10 and 4 hours of recording time,  
513 respectively).

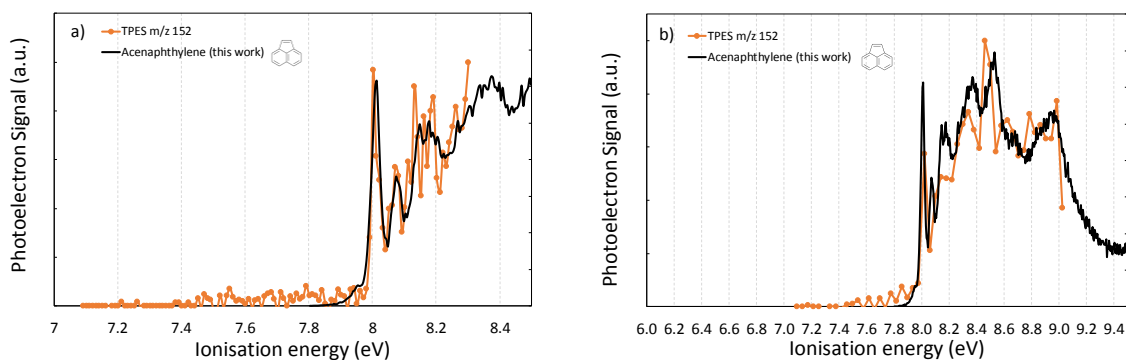
514

### 515 3.3.1 Analysis of the species at 152 m/z ( $C_{12}H_8$ )

516 This  $m/z$  is frequently detected in the mass spectra of rich and lightly sooting flames. The  
517 isomers commonly associated to this mass in the literature are 1-ethynyl-naphthalene  
518 ( $IE=8.03$  eV)<sup>95</sup>, 2-ethynyl-naphthalene ( $IE=8.11$  eV)<sup>95</sup>, biphenylene ( $IE=7.56$  eV)<sup>77</sup> and  
519 acenaphthylene ( $IE=8.02$  eV)<sup>76</sup>. PIE curves are often used for the identification of these species.  
520 However, the close ionization threshold values of these compounds do not allow the clear  
521 distinction of acenaphthylene and the two ethynyl-naphthalene isomers.

522 The vibronic structure seen in the TPES reported in **fig.7** provides much more precise  
523 information for the identification of these species. **Fig.7a** shows the TPES measured at HAB =  
524 9 mm while **fig.7b** shows the spectrum recorded at HAB = 15 mm. The TPES of pure  
525 acenaphthylene measured in this work (see **fig.2**) is shown alongside for comparison.

526



527

528 **Figure 7: TPES of 152 m/z at HAB = 9 and 15 mm.**

529 **Comparison with reference TPES of acenaphthylene.**

530

531 Both experiments show an excellent agreement between the TPES recorded in the flame and  
532 pure acenaphthylene. The TPES recorded at HAB = 9 mm with a smaller energy step shows  
533 vibrational modes clearly assignable to acenaphthylene. The second spectrum measured at  
534 HAB = 15 mm, over a broader energy scale but with larger energy steps, does not allow such a  
535 detailed analysis because of its lower resolution. However, the first very narrow vibrational

536 mode is still captured by the experiment and the recorded spectrum globally shows an excellent  
537 match with the overall shape of the pure acenaphthylene spectrum over this larger energy scale.  
538 These data clearly support acenaphthylene as the main species detected at 152  $m/z$  in the  
539 nucleation region of the flame.

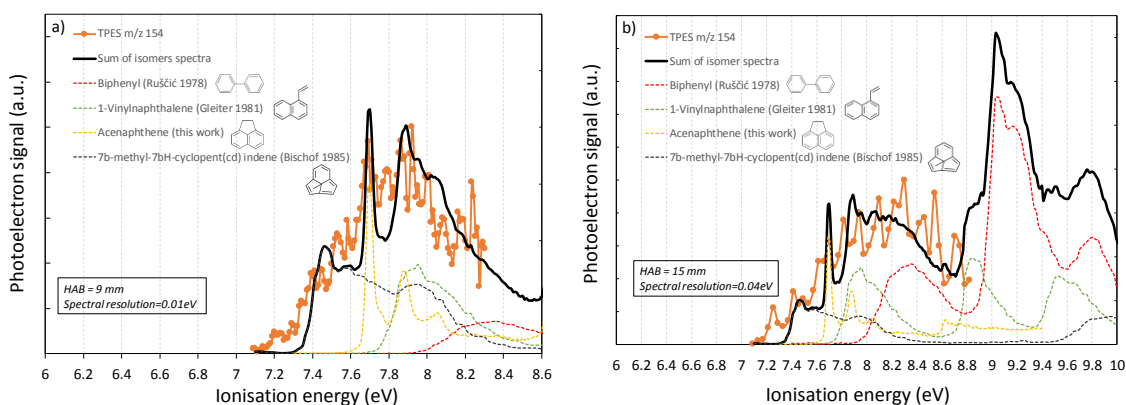
540

### 541 **3.3.2 Analysis of the species at 154 $m/z$ ( $C_{12}H_{10}$ )**

542 This mass is usually assigned, in rich flame studies reported the literature, to biphenyl  
543 ( $IE=8.16$  eV)<sup>37</sup> and acenaphthene ( $IE=7.67$  eV)<sup>37</sup>. We have reported in *fig.8a and fig.8b*, the  
544 TPES measured at HAB = 9 and 15 mm. These two spectra are relatively noisy in comparison to  
545 previous measurements at 152  $m/z$ . Moreover, the global structure of both spectra (HAB = 9 and  
546 15 mm) does not display any specific features as observed for other selected  $m/z$ , except a  
547 moderate peak around 7.70 eV. The absence of such peculiar spectral features illustrates the  
548 limitation of the TPEPICO method which may arise in some cases for the identification of  
549 structural isomers. However, these limitations would be even more severe with the use of PIE  
550 which would be totally featureless.

551 Hence, to interpret this spectrum, we first tried to reproduce it with a linear combination of  
552 the two commonly considered isomers in flames at 154  $m/z$  (biphenyl and acenaphthene) without  
553 success, meaning that some additional isomers were to be considered for this mass. However, we  
554 note an interesting match between the experimental peak detected around 7.70 eV and the first  
555 vibrational mode of the reference spectrum of acenaphthene that we determined (see *Fig.2*). To  
556 complete the overall structure of the simulated spectra, we checked in the literature<sup>37,96</sup> for other  
557 species corresponding to this mass, potentially formed in sooting flames.

558



559

560

**Figure 8: TPES of 154 m/z at HAB = 9 and 15 mm.**

561 **Comparison with a simulated spectrum (in black) corresponding to the sum of reference PES of biphenyl, 1-**  
 562 **vinylnaphthalene, acenaphthene and 7b-methyl-7bH-cyclopent(cd)indene for a signal ratio of 26:23:31:20 at**  
 563 **9 mm and 57:18:18:7 at 15 mm.**

564

565 Considering all the available spectra in databases<sup>37,96</sup>, we can only select two species, 1-  
 566 vinylnaphthalene ( $IE_{\text{vert}}=7.89$  eV) and 7b-methyl-7bH-cyclopent(cd)indene ( $IE_{\text{vert}}=7.56$  eV),  
 567 potentially matching some of the spectral features experimentally observed in our TPES. Among  
 568 these two species, 1-vinylnaphthalene is clearly expected to form in sooting flames according to  
 569 the HACA mechanism<sup>7</sup>. 7b-methyl-7bH-cyclopent(cd)indene, to the best of our knowledge, has  
 570 never been included in PAH growth models in rich flames. However, it was the only species  
 571 proposed in literature possessing a spectral structure peaking around 7.5 eV and thus matching  
 572 the first rising shape of the experimental spectrum. 1-vinylnaphthalene, despite being more  
 573 pertinent for soot formation and having an  $IE$  value estimated around 7.55 eV<sup>96</sup>, could not be  
 574 considered in the interpretation of the experimental data since no PES is currently available in  
 575 the literature.

576 Black spectra reported in **fig.8a** and **8b** correspond to the sum of the different contributions  
 577 of the individual spectra of the four considered species. The best matching signal ratio that  
 578 reproduces the experimental spectra at respective HAB = 9 and 15 mm are biphenyl (26% and  
 579 57%), 1-vinylnaphthalene (23% and 18%), acenaphthene (31% and 18%), 7b-methyl-7bH-

580 cyclopent(cd)indene (20% and 7%). However, caution must be exerted regarding the level of  
581 confidence in the identification. The most confident information from the comparison reported in  
582 *fig. 8a* is the formation of acenaphthene characterized by a very specific peak in the  
583 experimental spectrum matching the adiabatic transition of this compound around 7.70 eV and  
584 probably also the second peak around 7.85 eV. Conversely, this spectrum does not conclude on  
585 the formation of biphenyl at HAB = 9 mm. The main spectral features for this species are indeed  
586 located above 9 eV, that is slightly off the spectral range of the current experimental spectrum.  
587 However, the presence of biphenyl is more likely established on the less resolved TPES  
588 spectrum recorded at HAB = 15 mm. As can be seen, biphenyl is the only species with spectral  
589 features matching the shape of the spectrum between 8.2 and 8.8 eV. This part of the spectrum  
590 strongly evolves between 9 to 15 mm and might therefore correspond to the increase of the  
591 concentration of biphenyl with HAB. However, it is clear from the simulation that a spectrum  
592 registered on a larger spectral energy scale (up to 10 eV) would provide more conclusive  
593 information and confidence on the biphenyl formation, as well as having reference PES  
594 measured at higher resolution.

595 We can also note that the spectral features of 1-vinylnaphthalene match the experimental  
596 spectrum in *fig. 8a* between 7.8 and 8.2 eV. However, this spectral region is relatively large and  
597 does not display sufficient specific spectral features to allow a clear distinction of the species.

598 Finally, we have less confidence concerning the formation of 7b-methyl-7bH-  
599 cyclopent(cd)indene introduced in our simulated spectrum which appears atypical regarding  
600 published chemical analysis of sooting flames. It would have been more interesting to have the  
601 PES of 1-vinylnaphthalene which might also match the first spectral features of our TPES and is  
602 more expected to be formed in sooting flames.

603 Hence, the analysis for the detected mass 154  $m/z$ , although incomplete, nevertheless  
604 highlights the formation of several structural isomers in the nucleation region of the flame. It

605 clearly indicates the formation of acenaphthene and very probably of biphenyl and 1-  
606 vinylanthracene as well.

### 607 **3.3.3 Analysis of the species at 202 $m/z$ ( $C_{16}H_{10}$ )**

608 202  $m/z$  is usually attributed to pyrene in the analysis of sooting flames carried out by mass  
609 spectrometry. Pyrene is considered as a crucial species in soot formation process, and often  
610 proposed as a key molecule in the nucleation step leading to the inception of NSPs<sup>7,52,54,97-99</sup>. In  
611 previous works on the same flame<sup>25,53</sup>, we not only showed the formation of pyrene in the  
612 nucleation region of this flame, but also of fluoranthene. Both compounds have been identified  
613 by JCLIF<sup>25</sup>. The mole fractions of pyrene and fluoranthene in this flame have been determined  
614 by JCLIF as 0.36 ppm and 0.09 ppm at HAB = 9 mm, respectively, and 0.34 ppm and 0.12 ppm  
615 at HAB = 15 mm, respectively<sup>25</sup>.

616 Hence, the study of the 202  $m/z$  with the TPES setup is a meaningful benchmark to evaluate  
617 its sensitivity in this lightly sooting flame environment. We report in **fig.9** the TPES spectra  
618 measured at HAB = 9 and 15 mm with different spectral scan steps. We also report on these  
619 figures the calculated spectra (black line) corresponding to the sum of the adjusted contributions  
620 of the reference PES of pyrene (green dotted line) measured by Boschi et Schmidt<sup>100</sup> and  
621 fluoranthene (red dotted line) measured in this work (see **fig.2**). Moreover, we also considered  
622 the 9-ethynylphenanthrene (orange dotted line), also likely to form in this zone. We used for this  
623 species the referenced spectrum previously determined by Rouillé et al.<sup>74</sup>.

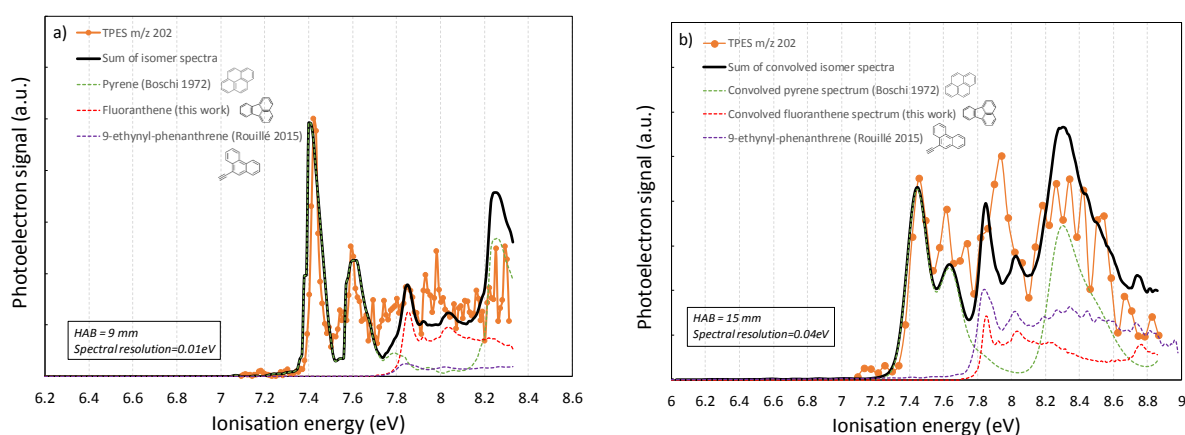
624 The relative contributions of pyrene and fluoranthene were adjusted for each HAB according  
625 to our previous mole fraction measurements in this flame by JCLIF. Based on these data, we  
626 obtained  $x_{\text{pyrene}}/x_{\text{fluoranthene}}=4$  at HAB = 9 mm and  $x_{\text{pyrene}}/x_{\text{fluoranthene}}=3$  at HAB = 15 mm. Finally,  
627 we adjusted the contribution of 9-ethynylphenanthrene to get the best agreement between the  
628 global simulated spectrum with the experimental one for each HAB. It should be noted that we  
629 slightly degraded the resolution of the pyrene and fluoranthene spectra to match the experimental

630 conditions of the spectrum recorded at HAB = 15 mm. Note also that this procedure assumes  
631 equal absolute ionization cross-sections for all structural isomers. This assumption is confirmed  
632 here by the good agreement obtained when using the mole fractions extracted from JCLIF to  
633 match the experimental TPES.

634 The comparison reported in *fig. 9a* provides an excellent agreement between the experimental  
635 spectrum and the simulated one obtained by adjusting the intensities of the pyrene and  
636 fluoranthene contributions with the value of the corresponding mole fractions determined  
637 previously<sup>25</sup>. This point hence validates the quantitative aspect of the TPES setup, providing  
638 experimental spectra with intensities proportional to the concentrations of the measured species.

639 The spectrum in *fig.9a* shows an excellent match of the two first sharp features of the  
640 experimental spectrum around 7.43 eV and 7.58 eV with the two first vibrational bands of  
641 pyrene PES. These values are in excellent agreement with the *IE* values (7.43 eV and 7.61 eV) of  
642 the pyrene reference spectrum<sup>100</sup>. This experiment therefore demonstrates that pyrene can be  
643 unambiguously identified by its PES measured with the TPES setup at this very low  
644 concentration.

645



646

647 **Figure 9: TPES spectra of 202 m/z at HAB = 9 and 15 mm.**

648 **Comparison with a simulated spectrum (in black) corresponding to the sum of reference PES of pyrene,**

649 **fluoranthene and 9-ethynyl-phenanthrene for a signal ratio of 77:19:4 at 9 mm and 56:18:26 at 15 mm.**

650

651 The section of the spectrum above 7.6 eV is noisier but still exhibits a structure that can be  
652 reproduced by the weighted sum of the pyrene and fluoranthene referenced PES. We can  
653 however note a slight shift between the value of the experimental (7.94 eV) and simulated (7.86  
654 eV) peak, corresponding to the *IE* of the first band of fluoranthene. This difference is attributed  
655 to the poor SNR in this zone of the spectrum due to the very weak mole fraction of fluoranthene  
656 ( $x_{\text{fluoranthene}} < 0.1$  ppm), and to the overlap of the spectral contributions of pyrene and  
657 fluoranthene. However, the experimental and simulated structures show a satisfying global  
658 match allowing the identification of both pyrene and fluoranthene. This comparison also shows a  
659 minor contribution of 9-ethynylphenanthrene to the overall spectral structure at HAB = 9 mm.  
660 The relative contributions we obtained this way were 77%, 19% and 4% respectively defining  
661 the pyrene, fluoranthene and 9-ethynylphenanthrene contributions, although detection of the  
662 latter is more speculative since its concentration would then be 0.01 ppm, well below our  
663 estimated detection limit.

664 The spectrum recorded at 15 mm exhibits a different structure because of the more important  
665 relative contribution of fluoranthene and 9-ethynylphenanthrene in comparison with pyrene in  
666 this region of the flame. Again, the contributions of pyrene and fluoranthene have been adjusted  
667 on previous JCLIF measurements at this HAB ( $x_{\text{pyrene}}/x_{\text{fluoranthene}}=3$ ), while the relative  
668 contribution of 9-ethynylphenanthrene has been adjusted to obtain the best fit of the  
669 experimental spectrum. The procedure leads to relative ratios of 56%, 18% and 26% for the  
670 pyrene, fluoranthene and 9-ethynylphenanthrene contributions, respectively. As seen in Fig. 9b,  
671 the experimental spectrum measured at 15 mm can still be correctly reproduced by the  
672 contributions of these three species and shows a strong increase of the contribution of the 9-  
673 ethynylphenanthrene. However, it would have been difficult to make this statement without the  
674 knowledge of the relative contributions of pyrene and fluoranthene deduced from previous



675 JCLIF measurements since fluoranthene and 9-ethynylphenanthrene have very similar spectra in  
676 this spectral range. Therefore, to gain confidence in the attribution, acquisition up to 10 eV  
677 seems mandatory, as it would allow considering spectral features in a zone with less overlap  
678 between the two species.

679 It should be noted that 202  $m/z$  has already been measured in rich or lightly sooting flames  
680 studies and generally attributed to pyrene alone<sup>31,82</sup> by the analysis of the PIE curves. However,  
681 in two recent papers, Johansson et al.<sup>35,101</sup> reported experimental PIE curves of 202  $m/z$  obtained  
682 from condensed species onto incipient soot particles and sampled from different ethylene flames.  
683 In these works, they concluded that their PIE curves could not be attributed to pyrene alone, and  
684 that the contribution of fluoranthene had also to be considered. Here, we reach the same  
685 conclusion for the gas phase. Interestingly, the adjusted contribution of these two PAHs (66%  
686 and 33%) determined by Johansson et al.<sup>35</sup> for the condensed species of 202  $m/z$  onto incipient  
687 soot particles is very similar to this work. This similarity is remarkable, considering the  
688 differences between these two flame setups (atmospheric pressure ethylene flame vs. low  
689 pressure methane flame).

690 Hence, TPES data confirm the formation of fluoranthene (and probably 9-  
691 ethynylphenanthrene) in addition to pyrene at 202  $m/z$ , and highlights their potential implication  
692 in the soot nucleation process, further reinforced by their presence as condensates onto incipient  
693 soot particles<sup>35,101</sup>.

694

### 695 **3.3.4 Analysis of the species at 226 $m/z$ ( $C_{18}H_{10}$ )**

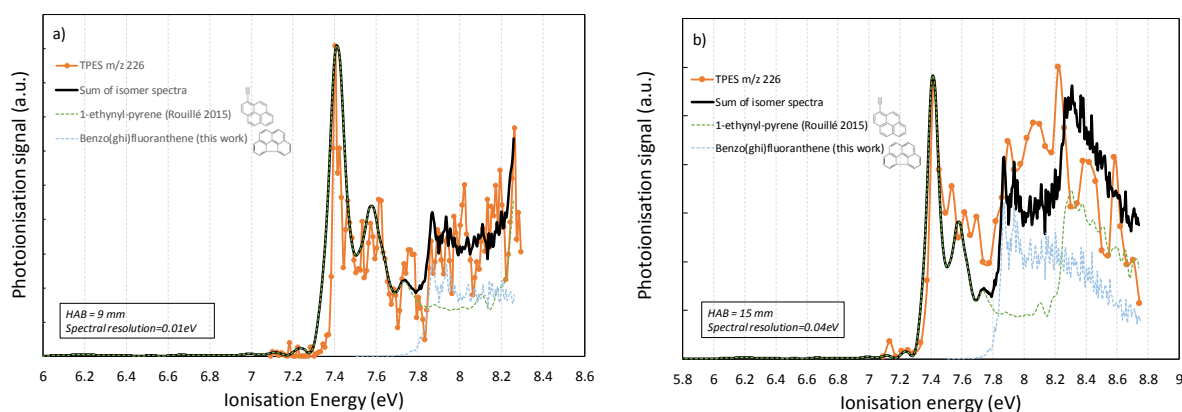
696 226  $m/z$  is often attributed to CP-PAHs likely involved in the soot nucleation process<sup>11,12,101</sup>.  
697 However, only a few analyses are reported in the literature and no clear attribution has ever been  
698 reported before. Several factors can explain the difficulty to analyze 226  $m/z$  as the large number  
699 of potential structural isomers and the lack of reference data such as *IE*, PIE curves or PES. To

700 date, only five out of the whole possible structural isomers are listed in the online NIST  
 701 database<sup>37</sup>, that furthermore only contains incomplete information: benzo[ghi]fluoranthene C1=CC=C2C=CC=CC=C2C3=CC=CC=C13,  
 702 cyclopenta[cd]-pyrene C1=CC=C2C=CC=CC=C2C3=CC=CC=C13, cyclopent[fg]aceanthrylene C1=CC=C2C=CC=CC=C2C3=CC=CC=C13 3,4-dihydrocyclopenta[cd]pyrene C1=CC=C2C=CC=CC=C2C3=CC=CC=C13  
 703 and benz[mno]aceanthrylene C1=CC=C2C=CC=CC=C2C3=CC=CC=C13. It is worth noting that all these candidates are CP-PAHs  
 704 containing a five-carbon ring in their structures. This lack of data makes therefore the  
 705 interpretation of 226  $m/z$  PES/TPES a very challenging task. In this work, we determined for the  
 706 first time, the TPES spectra of the benzo[ghi]fluoranthene to aid in the analysis of this peak.

707 Among the other potential candidates, we also considered the 1-ethynyl-pyrene C#CC1=CC=C2C=CC=CC=C2C3=CC=CC=C13, the  
 708 spectrum of which has been recorded by Rouillé et al.<sup>74</sup>

709 As for previous mass analyses, we report in **fig.10** the TPES corresponding to 226  $m/z$   
 710 measured with different spectral resolutions and over different energy ranges at HAB = 9 and 15  
 711 mm compared to the simulated spectrum obtained with the reference spectra of 1-ethynyl-pyrene  
 712 and benzo(ghi)fluoranthene.

713  
 714



715  
 716 **Figure 10: TPES of 226  $m/z$  at HAB = 9 and 15 mm.**  
 717 **Comparison with a simulated spectrum (in black) corresponding to the sum of reference PES of 1-ethynyl-pyrene**  
 718 **and benzo(ghi)fluoranthene for a signal ratio of 77:23 at 9 mm and 65:35 at 15 mm.**

719  
720 As seen in *fig. 10a*, the experimental and simulated spectra are in excellent agreement by  
721 considering only 1-ethynyl-pyrene and benzo(ghi)fluoranthene. An excellent match of the two  
722 first peaks of the experimental structure with the first two vibrational bands of 1-ethynyl-pyrene,  
723 peaking at 7.41 and 7.58 eV, is observed. The second part of the spectrum is noisier but also  
724 shows an excellent agreement with the adjusted contributions of both 1-ethynyl-pyrene and  
725 benzo(ghi)fluoranthene. We reached the best agreement by adjusting the relative signal  
726 contribution of 1-ethynyl-pyrene and benzo(ghi)fluoranthene equal to 77% and 23%. The  
727 spectrum recorded at HAB = 15 mm over a larger energy range still provides an adequate  
728 spectral resolution to identify these two species. The first peak of the spectrum is notably in  
729 perfect agreement with the energy of the first vibrational band of 1-ethynyl-pyrene. The rest of  
730 the spectrum is globally correctly reproduced by the simulated structure by considering relative  
731 contributions of 1-ethynyl-pyrene and benzo(ghi)fluoranthene equal to 65% and 35%. These data  
732 show again that CP-PAH and substituted PAHs actively occur in the nucleation region of the  
733 flame.

734 Recently, Adamson et al.<sup>102</sup> reported experiments, carried out with a tandem mass  
735 spectrometer, showing the formation of aliphatically bridged structures in an ethylene/O<sub>2</sub> coflow  
736 diffusion flame. These structures, constituted of PAHs bonded by a carbon chain, are suggested  
737 as a particle seeds in sooting flames. Their formation would be based on a growth mechanism  
738 involving side-substituted aromatics formed through reactions of smaller aromatic species and  
739 aliphatic hydrocarbons. In this work, Adamson et al.<sup>102</sup> notably detected the species C<sub>18</sub>H<sub>10</sub> at  
740 226 *m/z* as a very stable building block. The information provided in this work in the nucleation  
741 zone, complementary highlights the formation of a side-substituted PAH as part of the  
742 compounds detected at this mass and therefore their possible involvement in the formation of  
743 such aliphatically-bridged PAHs. Furthermore, recent studies suggested that these compounds

744 would be stable enough to resist in flame conditions<sup>103</sup> and might be at the origin of the  
745 broadband fluorescence emission spectra commonly observed in such sooting flames by laser  
746 excitation<sup>23,104</sup> in the nucleation zone.

747

748

749

#### 750 **4 Conclusion**

751 This work demonstrates and benchmarks the capabilities of the multiplex *i*<sup>2</sup>PEPICO  
752 technique to study sooting flames. Mass-selected PES and TPES spectra corresponding to  
753 different PAHs have been reported for samples obtained at different heights above the burner in  
754 a sooting low-pressure methane flame. The identification of structural isomers at each *m/z*  
755 channel relies on the comparison of the recorded experimental spectra with reference PES, which  
756 act as molecular fingerprints. From this work, it appears that the analysis of the TPES spectra  
757 enables the accurate identification of the PAHs formed in the flame. The PES, which are  
758 recorded at fixed photon energies with much shorter acquisition time than TPES scans, present a  
759 less accurate resolution and lower SNR. However, these spectra have been shown for the  
760 smallest species, at least up to naphthalene, to be sufficiently resolved to capture the main  
761 electronic features of the PAHs and in some cases, even the vibrational progressions. However,  
762 for the largest PAHs with concentrations below the ppm, we observed that only the TPES  
763 approach provided sufficient sensitivity and spectral selectivity to enable the identification of the  
764 different structural isomers.

765 This study provides evidence of the formation of CP-PAHs in the nucleation zone of the  
766 sooting flame, such as indene, acenaphthylene, fluoranthene and benzo(ghi)fluoranthene. Such  
767 CP-PAHs likely correspond to the cyclopentaring observed in the curved graphene layer present  
768 in the core region of soot particles<sup>55</sup>. Moreover, we also highlight the presence of side-

769 substituted aromatics besides CP-PAHs which have been recently suggested to lead to the  
770 formation of aliphatically bridged structures which could serve as a particle seed<sup>102</sup>. This work  
771 emphasizes the importance of considering the chemical pathways and overall kinetics leading to  
772 the formation of CP-PAHs and side-substituted aromatics in the development of soot formation  
773 mechanisms<sup>57</sup>.

774 This first attempt of using the PEPICO setup of the DESIRS beamline at SOLEIL for the  
775 study of low pressure sooting premixed flames therefore appears very encouraging and shows a  
776 high potential for understanding in situ the mechanisms of soot and PAHs formation in  
777 laboratory flames. Means of improvement include the recording of higher quality PES to feed the  
778 current database—to which this work has already contributed with the reporting of the PES of  
779 acenaphthene, acenaphthylene, fluoranthene and benzo(ghi)fluoranthene—or the challenging  
780 measurement or calculation of absolute cross-sections to increase the quantitative potential of  
781 this method. The sensitivity of the setup, although adequate, might be improved to provide a  
782 better identification of PAH isomers by increasing the molecular beam density in the ionization  
783 region (shortening the nozzle-synchrotron beam distance, improving the gas inlet). However, we  
784 showed that the capabilities of the current setup already enable the possibility of more systematic  
785 studies aiming at the determination of experimental profiles of moderate size PAHs isomers  
786 involved in the soot formation process in flames. A deeper understanding of the soot nucleation  
787 process will require, at some point in the future, extending the measurements shown in this paper  
788 to the particulate phase at the very beginning of the soot formation. In this context, the use of the  
789 SAPHIRS chamber dedicated aerodynamic lens system, coupled to a thermodesorbing tip, could  
790 enable the measurements of the detailed chemical composition of nascent soot particles<sup>46</sup>.

791

792 **Acknowledgements**

793 This work is a contribution to the labex CAPP and the CPER research project CLIMIBIO. The  
794 authors thank the French Ministère de l'Enseignement Supérieur et de la Recherche, the Hauts de  
795 France Region and the European Funds for Regional Economical Development for their  
796 financial support to this project." We are grateful to J.-F. Gil for his technical help around the  
797 SAPHIRS set-up. We warmly thank the whole SOLEIL staff for running the facility and  
798 providing beamtime under project number 20151078 and 20170070.

799

800

801

## 802 **References**

- 803 1 J. C. Chow, Health Effects of Fine Particulate Air Pollution: Lines that Connect, *Journal of*  
804 *the Air & Waste Management Association*, 2006, **56**, 707–708.
- 805 2 T. Petry, P. Schmid and C. Schlatter, The use of toxic equivalency factors in assessing  
806 occupational and environmental health risk associated with exposure to airborne mixtures of  
807 polycyclic aromatic hydrocarbons (PAHs), *Chemosphere*, 1996, **32**, 639–648.
- 808 3 R. Niranjana and A. K. Thakur, The Toxicological Mechanisms of Environmental Soot (Black  
809 Carbon) and Carbon Black: Focus on Oxidative Stress and Inflammatory Pathways, *Front.*  
810 *Immunol.*, , DOI:10.3389/fimmu.2017.00763.
- 811 4 S. S. Lim, T. Vos, A. D. Flaxman, G. Danaei, K. Shibuya, H. Adair-Rohani, M. A. AlMazroa,  
812 M. Amann, H. R. Anderson, K. G. Andrews, M. Aryee, C. Atkinson, L. J. Bacchus, A. N.  
813 Bahalim, K. Balakrishnan, J. Balmes, S. Barker-Collo, A. Baxter, M. L. Bell, J. D. Blore, F.  
814 Blyth, C. Bonner, G. Borges, R. Bourne, M. Boussinesq, M. Brauer, P. Brooks, N. G. Bruce,  
815 B. Brunekreef, C. Bryan-Hancock, C. Bucello, R. Buchbinder, F. Bull, R. T. Burnett, T. E.  
816 Byers, B. Calabria, J. Carapetis, E. Carnahan, Z. Chafe, F. Charlson, H. Chen, J. S. Chen, A.  
817 T.-A. Cheng, J. C. Child, A. Cohen, K. E. Colson, B. C. Cowie, S. Darby, S. Darling, A.  
818 Davis, L. Degenhardt, F. Dentener, D. C. Des Jarlais, K. Devries, M. Dherani, E. L. Ding, E.  
819 R. Dorsey, T. Driscoll, K. Edmond, S. E. Ali, R. E. Engell, P. J. Erwin, S. Fahimi, G. Falder,  
820 F. Farzadfar, A. Ferrari, M. M. Finucane, S. Flaxman, F. G. R. Fowkes, G. Freedman, M. K.  
821 Freeman, E. Gakidou, S. Ghosh, E. Giovannucci, G. Gmel, K. Graham, R. Grainger, B. Grant,  
822 D. Gunnell, H. R. Gutierrez, W. Hall, H. W. Hoek, A. Hogan, H. D. Hosgood, D. Hoy, H. Hu,  
823 B. J. Hubbell, S. J. Hutchings, S. E. Ibeanusi, G. L. Jacklyn, R. Jasrasaria, J. B. Jonas, H. Kan,  
824 J. A. Kanis, N. Kassebaum, N. Kawakami, Y.-H. Khang, S. Khatibzadeh, J.-P. Khoo, C. Kok,  
825 F. Laden, R. Lalloo, Q. Lan, T. Lathlean, J. L. Leasher, J. Leigh, Y. Li, J. K. Lin, S. E.  
826 Lipshultz, S. London, R. Lozano, Y. Lu, J. Mak, R. Malekzadeh, L. Mallinger, W. Marcenes,  
827 L. March, R. Marks, R. Martin, P. McGale, J. McGrath, S. Mehta, Z. A. Memish, G. A.  
828 Mensah, T. R. Merriman, R. Micha, C. Michaud, V. Mishra, K. M. Hanafiah, A. A. Mokdad,  
829 L. Morawska, D. Mozaffarian, T. Murphy, M. Naghavi, B. Neal, P. K. Nelson, J. M. Nolla, R.  
830 Norman, C. Olives, S. B. Omer, J. Orchard, R. Osborne, B. Ostro, A. Page, K. D. Pandey, C.  
831 D. Parry, E. Passmore, J. Patra, N. Pearce, P. M. Pelizzari, M. Petzold, M. R. Phillips, D.  
832 Pope, C. A. Pope, J. Powles, M. Rao, H. Razavi, E. A. Rehfuss, J. T. Rehm, B. Ritz, F. P.

- 833 Rivara, T. Roberts, C. Robinson, J. A. Rodriguez-Portales, I. Romieu, R. Room, L. C.  
834 Rosenfeld, A. Roy, L. Rushton, J. A. Salomon, U. Sampson, L. Sanchez-Riera, E. Sanman, A.  
835 Sapkota, S. Seedat, P. Shi, K. Shield, R. Shivakoti, G. M. Singh, D. A. Sleet, E. Smith, K. R.  
836 Smith, N. J. Stapelberg, K. Steenland, H. Stöckl, L. J. Stovner, K. Straif, L. Straney, G. D.  
837 Thurston, J. H. Tran, R. Van Dingenen, A. van Donkelaar, J. L. Veerman, L. Vijayakumar, R.  
838 Weintraub, M. M. Weissman, R. A. White, H. Whiteford, S. T. Wiersma, J. D. Wilkinson, H.  
839 C. Williams, W. Williams, N. Wilson, A. D. Woolf, P. Yip, J. M. Zielinski, A. D. Lopez, C. J.  
840 Murray and M. Ezzati, A comparative risk assessment of burden of disease and injury  
841 attributable to 67 risk factors and risk factor clusters in 21 regions, 1990–2010: a systematic  
842 analysis for the Global Burden of Disease Study 2010, *The Lancet*, 2012, **380**, 2224–2260.
- 843 5 T. C. Bond, S. J. Doherty, D. W. Fahey, P. M. Forster, T. Berntsen, B. J. DeAngelo, M. G.  
844 Flanner, S. Ghan, B. Kärcher, D. Koch, S. Kinne, Y. Kondo, P. K. Quinn, M. C. Sarofim, M.  
845 G. Schultz, M. Schulz, C. Venkataraman, H. Zhang, S. Zhang, N. Bellouin, S. K. Guttikunda,  
846 P. K. Hopke, M. Z. Jacobson, J. W. Kaiser, Z. Klimont, U. Lohmann, J. P. Schwarz, D.  
847 Shindell, T. Storelvmo, S. G. Warren and C. S. Zender, Bounding the role of black carbon in  
848 the climate system: A scientific assessment, *Journal of Geophysical Research: Atmospheres*,  
849 2013, **118**, 5380–5552.
- 850 6 B. Gorbunov, A. Baklanov, N. Kakutkina, H. L. Windsor and R. Toumi, Ice nucleation on  
851 soot particles, *Journal of Aerosol Science*, 2001, **32**, 199–215.
- 852 7 M. Frenklach and H. Wang, Detailed modeling of soot particle nucleation and growth,  
853 *Symposium (International) on Combustion*, 1991, **23**, 1559–1566.
- 854 8 A. D’Anna, *Combustion Generated Fine Carbonaceous Particles*, KIT Scientific Publishing,  
855 Karlsruhe, 2009.
- 856 9 A. D’Anna, Combustion-formed nanoparticles, *Proceedings of the Combustion Institute*,  
857 2009, **32**, 593–613.
- 858 10 H. Wang, Formation of nascent soot and other condensed-phase materials in flames,  
859 *Proceedings of the Combustion Institute*, 2011, **33**, 41–67.
- 860 11 B. Shukla and M. Koshi, A novel route for PAH growth in HACA based mechanisms,  
861 *Combustion and Flame*, 2012, **159**, 3589–3596.
- 862 12 B. Shukla and M. Koshi, Comparative study on the growth mechanisms of PAHs, *Combustion*  
863 *and Flame*, 2011, **158**, 369–375.
- 864 13 C. S. McEnally, L. D. Pfefferle, B. Atakan and K. Kohse-Höinghaus, Studies of aromatic  
865 hydrocarbon formation mechanisms in flames: Progress towards closing the fuel gap,  
866 *Progress in Energy and Combustion Science*, 2006, **32**, 247–294.
- 867 14 M. Commodo, K. Kaiser, G. De Falco, P. Minutolo, F. Schulz, A. D’Anna and L. Gross, On  
868 the early stages of soot formation: Molecular structure elucidation by high-resolution atomic  
869 force microscopy, *Combustion and Flame*, 2019, **205**, 154–164.
- 870 15 K. Siegmann and K. Sattler, Formation mechanism for polycyclic aromatic hydrocarbons in  
871 methane flames, *J. Chem. Phys.*, 1999, **112**, 698–709.
- 872 16 J. Xiao, E. Austin and W. L. Roberts, Relative Polycyclic Aromatic Hydrocarbon  
873 Concentrations in Unsteady Counterflow Diffusion Flames, *Combustion Science and*  
874 *Technology*, 2005, **177**, 691–713.
- 875 17 S. Bejaoui, X. Mercier, P. Desgroux and E. Therssen, Laser induced fluorescence  
876 spectroscopy of aromatic species produced in atmospheric sooting flames using UV and  
877 visible excitation wavelengths, *Combustion and Flame*, 2014, **161**, 2479–2491.
- 878 18 K. C. Smyth, C. R. Shaddix and D. A. Everest, Aspects of soot dynamics as revealed by  
879 measurements of broadband fluorescence and flame luminosity in flickering diffusion flames,  
880 *Combustion and Flame*, 1997, **111**, 185–207.
- 881 19 S.-Y. Lee, S. R. Turns and R. J. Santoro, Measurements of soot, OH, and PAH concentrations  
882 in turbulent ethylene/air jet flames, *Combustion and Flame*, 2009, **156**, 2264–2275.

- 883 20M. Köhler, K. P. Geigle, T. Blacha, P. Gerlinger and W. Meier, Experimental characterization  
884 and numerical simulation of a sooting lifted turbulent jet diffusion flame, *Combustion and*  
885 *Flame*, 2012, **159**, 2620–2635.
- 886 21 A. Ciajolo, R. Ragucci, B. Apicella, R. Barbella, M. de Joannon and A. Tregrossi,  
887 Fluorescence spectroscopy of aromatic species produced in rich premixed ethylene flames,  
888 *Chemosphere*, 2001, **42**, 835–841.
- 889 22M. Sirignano, A. Collina, M. Commodo, P. Minutolo and A. D’Anna, Detection of aromatic  
890 hydrocarbons and incipient particles in an opposed-flow flame of ethylene by spectral and  
891 time-resolved laser induced emission spectroscopy, *Combustion and Flame*, 2012, **159**, 1663–  
892 1669.
- 893 23X. Mercier, O. Carrivain, C. Irimiea, A. Faccinnetto and E. Therssen, Dimers of polycyclic  
894 aromatic hydrocarbons: the missing pieces in the soot formation process, *Phys. Chem. Chem.*  
895 *Phys.*, 2019, **21**, 8282–8294.
- 896 24Y. Zhang, Y. Li, L. Wang, P. Liu, R. Zhan, Z. Huang and H. Lin, Investigation on the LIF  
897 spectrum superposition of gas-phase PAH mixtures at elevated temperatures: potential for the  
898 analysis of PAH LIF spectra in sooting flames, *Appl. Phys. B*, 2019, **125**, 72.
- 899 25T. Mouton, X. Mercier and P. Desgroux, Isomer discrimination of PAHs formed in sooting  
900 flames by jet-cooled laser-induced fluorescence: application to the measurement of pyrene  
901 and fluoranthene, *Applied Physics B*, 2016, **122**, 123–139.
- 902 26X. Mercier, M. Wartel, J.-F. Pauwels and P. Desgroux, Implementation of a new  
903 spectroscopic method to quantify aromatic species involved in the formation of soot particles  
904 in flames, *Applied Physics B: Lasers and Optics*, 2008, **91**, 387–395.
- 905 27C. A. Taatjes, N. Hansen, D. L. Osborn, K. Kohse-Hoinghaus, T. A. Cool and P. R.  
906 Westmoreland, “Imaging” combustion chemistry via multiplexed synchrotron-photoionization  
907 mass spectrometry, *Physical Chemistry Chemical Physics*, 2008, **10**, 20–34.
- 908 28F. Qi, R. Yang, B. Yang, C. Huang, L. Wei, J. Wang, L. Sheng and Y. Zhang, Isomeric  
909 identification of polycyclic aromatic hydrocarbons formed in combustion with tunable  
910 vacuum ultraviolet photoionization, *Review of Scientific Instruments*, 2006, **77**, 084101.
- 911 29L. Zhao, R. I. Kaiser, B. Xu, U. Ablikim, M. Ahmed, D. Joshi, G. Veber, F. R. Fischer and A.  
912 M. Mebel, Pyrene synthesis in circumstellar envelopes and its role in the formation of 2D  
913 nanostructures, 2018, **2**, 413–419.
- 914 30F. Qi, Combustion Chemistry Probed by Synchrotron VUV Photo-ionization Mass  
915 Spectrometry, *Proceedings of the Combustion Institute*, 2013, **34**, 33–63.
- 916 31Y. Li, L. Zhang, Z. Tian, T. Yuan, J. Wang, B. Yang and F. Qi, Experimental Study of a Fuel-  
917 Rich Premixed Toluene Flame at Low Pressure, *Energy Fuels*, 2009, **23**, 1473–1485.
- 918 32Y. Li, Z. Tian, L. Zhang, T. Yuan, K. Zhang, B. Yang and F. Qi, An experimental study of the  
919 rich premixed ethylbenzene flame at low pressure, *Proceedings of the Combustion Institute*,  
920 2009, **32**, 647–655.
- 921 33Y. Li, L. Zhang, Z. Tian, T. Yuan, K. Zhang, B. Yang and F. Qi, Investigation of the rich  
922 premixed laminar acetylene/oxygen/argon flame: Comprehensive flame structure and special  
923 concerns of polyynes, *Proceedings of the Combustion Institute*, 2009, **32**, 1293–1300.
- 924 34B. Yang, Y. Li, L. Wei, C. Huang, J. Wang, Z. Tian, R. Yang, L. Sheng, Y. Zhang and F. Qi,  
925 An experimental study of the premixed benzene/oxygen/argon flame with tunable synchrotron  
926 photoionization, *Proceedings of the Combustion Institute*, 2007, **31**, 555–563.
- 927 35K. O. Johansson, J. Zádor, P. Elvati, M. F. Campbell, P. E. Schrader, N. K. Richards-  
928 Henderson, K. R. Wilson, A. Violi and H. A. Michelsen, Critical Assessment of  
929 Photoionization Efficiency Measurements for Characterization of Soot-Precursor Species, *J.*  
930 *Phys. Chem. A*, 2017, **121**, 4475–4485.
- 931 36T. Zhang, L. Zhang, X. Hong, K. Zhang, F. Qi, C. K. Law, T. Ye, P. Zhao and Y. Chen, An  
932 experimental and theoretical study of toluene pyrolysis with tunable synchrotron VUV



- 933 photoionization and molecular-beam mass spectrometry, *Combustion and Flame*, 2009, **156**,  
934 2071–2083.
- 935 37 S. G. Lias, in *NIST Chemistry WebBook, NIST Standard Reference Database Number 69*,  
936 edited by P. J. Linstrom and W. G. Mallard (National Institute of Standards and Technology,  
937 Gaithersburg, MD), 20899. <http://webbook.nist.gov/chemistry/>. Accessed 26 November 2012,  
938 2012.
- 939 38 P. Bréchnignac, G. A. Garcia, C. Falvo, C. Joblin, D. Kokkin, A. Bonnamy, P. Parneix, T.  
940 Pino, O. Pirali, G. Mulas and L. Nahon, Photoionization of cold gas phase coronene and its  
941 clusters: Autoionization resonances in monomer, dimer, and trimer and electronic structure of  
942 monomer cation, *J. Chem. Phys.*, 2014, **141**, 164325.
- 943 39 P. Oßwald, P. Hemberger, T. Bierkandt, E. Akyildiz, M. Köhler, A. Bodi, T. Gerber and T.  
944 Kasper, In situ flame chemistry tracing by imaging photoelectron photoion coincidence  
945 spectroscopy, *Review of Scientific Instruments*, 2014, **85**, 025101.
- 946 40 D. Felsmann, K. Moshhammer, J. Krüger, A. Lackner, A. Brockhinke, T. Kasper, T. Bierkandt,  
947 E. Akyildiz, N. Hansen, A. Lucassen, P. Oßwald, M. Köhler, G. A. Garcia, L. Nahon, P.  
948 Hemberger, A. Bodi, T. Gerber and K. Kohse-Höinghaus, Electron ionization, photoionization  
949 and photoelectron/photoion coincidence spectroscopy in mass-spectrometric investigations of  
950 a low-pressure ethylene/oxygen flame, *Proceedings of the Combustion Institute*, 2015, **35**,  
951 779–786.
- 952 41 D. Felsmann, A. Lucassen, J. Krüger, C. Hemken, L.-S. Tran, J. Pieper, G. A. Garcia, A.  
953 Brockhinke, L. Nahon and K. Kohse-Höinghaus, Progress in Fixed-Photon-Energy Time-  
954 Efficient Double Imaging Photoelectron/Photoion Coincidence Measurements in Quantitative  
955 Flame Analysis, *Zeitschrift für Physikalische Chemie*, 2016, **230**, 1067–1097.
- 956 42 J. Pieper, S. Schmitt, C. Hemken, E. Davies, J. Wullenkord, A. Brockhinke, J. Krüger, G. A.  
957 Garcia, L. Nahon, A. Lucassen, W. Eisfeld and K. Kohse-Höinghaus, Isomer Identification in  
958 Flames with Double-Imaging Photoelectron/Photoion Coincidence Spectroscopy (i2PEPICO)  
959 using Measured and Calculated Reference Photoelectron Spectra, *Zeitschrift für Physikalische  
960 Chemie*, 2018, **232**, 153–187.
- 961 43 J. Krüger, G. A. Garcia, D. Felsmann, K. Moshhammer, A. Lackner, A. Brockhinke, L. Nahon  
962 and K. Kohse-Höinghaus, Photoelectron–photoion coincidence spectroscopy for multiplexed  
963 detection of intermediate species in a flame, *Phys. Chem. Chem. Phys.*, 2014, **16**, 22791–  
964 22804.
- 965 44 P. Hemberger, V. B. F. Custodis, A. Bodi, T. Gerber and J. A. van Bokhoven, Understanding  
966 the mechanism of catalytic fast pyrolysis by unveiling reactive intermediates in heterogeneous  
967 catalysis, *Nat Commun*, 2017, **8**, 1–9.
- 968 45 D. Krüger, P. Oßwald, M. Köhler, P. Hemberger, T. Bierkandt, Y. Karakaya and T. Kasper,  
969 Hydrogen abstraction ratios: A systematic iPEPICO spectroscopic investigation in laminar  
970 flames, *Combustion and Flame*, 2018, **191**, 343–352.
- 971 46 M. T. Baeza-Romero, F. Gaie-Levrel, A. Mahjoub, V. López-Arza, G. A. Garcia and L.  
972 Nahon, A smog chamber study coupling a photoionization aerosol electron/ion spectrometer  
973 to VUV synchrotron radiation: organic and inorganic-organic mixed aerosol analysis, *Eur.  
974 Phys. J. D*, 2016, **70**, 154.
- 975 47 J. Bourgalais, Z. Gouid, O. Herbinet, G. A. Garcia, P. Arnoux, Z. Wang, L.-S. Tran, G.  
976 Vanhove, M. Hochlaf, L. Nahon and F. Battin-Leclerc, Isomer-sensitive characterization of  
977 low temperature oxidation reaction products by coupling a jet-stirred reactor to an electron/ion  
978 coincidence spectrometer: case of n-pentane, *Phys. Chem. Chem. Phys.*, 2020, **22**, 1222–1241.
- 979 48 A. Bodi, P. Hemberger, D. L. Osborn and B. Sztáray, Mass-Resolved Isomer-Selective  
980 Chemical Analysis with Imaging Photoelectron Photoion Coincidence Spectroscopy, *J. Phys.  
981 Chem. Lett.*, 2013, **4**, 2948–2952.

- 982 49 M. Wartel, J.-F. Pauwels, P. Desgroux and X. Mercier, Pyrene Measurements in Sooting Low  
983 Pressure Methane Flames by Jet-Cooled Laser-Induced Fluorescence, *Journal of Physical*  
984 *Chemistry A*, 2011, **115**, 14153–14162.
- 985 50 H. Bladh, N.-E. Olofsson, T. Mouton, J. Simonsson, X. Mercier, A. Faccinnetto, P.-E.  
986 Bengtsson and P. Desgroux, Probing the smallest soot particles in low-sooting premixed  
987 flames using laser-induced incandescence, *Proceedings of the Combustion Institute*, 2015, **35**,  
988 1843–1850.
- 989 51 T. Mouton, X. Mercier, M. Wartel, N. Lamoureux and P. Desgroux, Laser-induced  
990 incandescence technique to identify soot nucleation and very small particles in low-pressure  
991 methane flames, *Applied Physics B: Lasers and Optics*, 2013, **112**, 369–379.
- 992 52 A. El Bakali, X. Mercier, M. Wartel, F. Acevedo, I. S. Burns, L. Gasnot, J.-F. Pauwels and P.  
993 Desgroux, Modeling of PAHs in low pressure sooting premixed methane flame, *Energy*,  
994 2012, **43**, 73–84.
- 995 53 P. Desgroux, A. Faccinnetto, X. Mercier, T. Mouton, D. Aubagnac Karkar and A. El Bakali,  
996 Comparative study of the soot formation process in a “nucleation” and a “sooting” low  
997 pressure premixed methane flame, *Combustion and Flame*, 2017, **184**, 153–166.
- 998 54 D. Aubagnac-Karkar, A. El Bakali and P. Desgroux, Soot particles inception and PAH  
999 condensation modelling applied in a soot model utilizing a sectional method, *Combustion and*  
1000 *Flame*, 2018, **189**, 190–206.
- 1001 55 J.-O. Müller, D. S. Su, U. Wild and R. Schlögl, Bulk and surface structural investigations of  
1002 diesel engine soot and carbon black, *Phys. Chem. Chem. Phys.*, 2007, **9**, 4018–4025.
- 1003 56 M. Wei, T. Zhang, X. Chen, F. Yan, G. Guo and D. Zhang, Formation of bicyclic polycyclic  
1004 aromatic hydrocarbons (PAHs) from the reaction of a phenyl radical with cis-3-penten-1-yne,  
1005 *RSC Adv.*, 2018, **8**, 13226–13236.
- 1006 57 M. Frenklach and A. M. Mebel, On the mechanism of soot nucleation, *Phys. Chem. Chem.*  
1007 *Phys.*, 2020, **22**, 5314–5331.
- 1008 58 R. A. Krueger and G. Blanquart, Predicting the photoresponse of soot nuclei: Spectroscopic  
1009 characteristics of aromatic aggregates containing five-membered rings, *Combustion and*  
1010 *Flame*, 2020, **217**, 85–92.
- 1011 59 M. Tia, B. Cunha de Miranda, S. Daly, F. Gaie-Levrel, G. A. Garcia, I. Powis and L. Nahon,  
1012 Chiral Asymmetry in the Photoionization of Gas-Phase Amino-Acid Alanine at Lyman- $\alpha$   
1013 Radiation Wavelength, *J. Phys. Chem. Lett.*, 2013, **4**, 2698–2704.
- 1014 60 X. Tang, G. A. Garcia, J.-F. Gil and L. Nahon, Vacuum upgrade and enhanced performances  
1015 of the double imaging electron/ion coincidence end-station at the vacuum ultraviolet beamline  
1016 DESIRS, *Review of Scientific Instruments*, 2015, **86**, 123108.
- 1017 61 L. Nahon, N. de Oliveira, G. A. Garcia, J.-F. Gil, B. Pilette, O. Marcouillé, B. Lagarde and F.  
1018 Polack, DESIRS: a state-of-the-art VUV beamline featuring high resolution and variable  
1019 polarization for spectroscopy and dichroism at SOLEIL, *J Synchrotron Rad*, 2012, **19**, 508–  
1020 520.
- 1021 62 B. Mercier, M. Compin, C. Prevost, G. Bellec, R. Thissen, O. Dutuit and L. Nahon,  
1022 Experimental and theoretical study of a differentially pumped absorption gas cell used as a  
1023 low energy-pass filter in the vacuum ultraviolet photon energy range, *Journal of Vacuum*  
1024 *Science & Technology A*, 2000, **18**, 2533–2541.
- 1025 63 K. Yoshino and Y. Tanaka, Absorption spectrum of krypton in the vacuum uv region, *J. Opt.*  
1026 *Soc. Am., JOS A*, 1979, **69**, 159–165.
- 1027 64 G. A. Garcia, B. K. Cunha de Miranda, M. Tia, S. Daly and L. Nahon, DELICIOUS III: a  
1028 multipurpose double imaging particle coincidence spectrometer for gas phase vacuum  
1029 ultraviolet photodynamics studies, *Rev Sci Instrum*, 2013, **84**, 053112.
- 1030 65 G. A. Garcia, X. Tang, J.-F. Gil, L. Nahon, M. Ward, S. Batut, C. Fittschen, C. A. Taatjes, D.  
1031 L. Osborn and J.-C. Loison, Synchrotron-based double imaging photoelectron/photoion

- 1032 coincidence spectroscopy of radicals produced in a flow tube: OH and OD, *J. Chem. Phys.*,  
 1033 2015, **142**, 164201.
- 1034 66J. C. Pouilly, J. P. Schermann, N. Nieuwjaer, F. Lecomte, G. Grégoire, C. Desfrancois, G.  
 1035 A. Garcia, L. Nahon, D. Nandi, L. Poisson and M. Hochlaf, Photoionization of 2-pyridone and  
 1036 2-hydroxypyridine, *Physical Chemistry Chemical Physics*, 2010, **12**, 3566–3572.
- 1037 67M. Wartel, J.-F. Pauwels, P. Desgroux and X. Mercier, Quantitative measurement of  
 1038 naphthalene in low-pressure flames by jet-cooled laser-induced fluorescence, *Applied Physics*  
 1039 *B: Lasers and Optics*, 2010, **100**, 933–943.
- 1040 68T. S. Kasper, P. Oßwald, M. Kamphus and K. Kohse-Höinghaus, Ethanol flame structure  
 1041 investigated by molecular beam mass spectrometry, *Combustion and Flame*, 2007, **150**, 220–  
 1042 231.
- 1043 69N. Hansen, T. Kasper, S. J. Klippenstein, P. R. Westmoreland, M. E. Law, C. A. Taatjes, K.  
 1044 Kohse-Höinghaus, J. Wang and T. A. Cool, Initial Steps of Aromatic Ring Formation in a  
 1045 Laminar Premixed Fuel-Rich Cyclopentene Flame, *Journal of Physical Chemistry A*, 2007,  
 1046 **111**, 4081–4092.
- 1047 70H.-S. Kim, D. R. Wagner and R. J. Saykally, Single Photon Infrared Emission Spectroscopy  
 1048 of the Gas Phase Pyrene Cation: Support for a Polycyclic Aromatic Hydrocarbon Origin of  
 1049 the Unidentified Infrared Emission Bands, *Phys. Rev. Lett.*, 2001, **86**, 5691–5694.
- 1050 71J. E. Elsila, N. P. de Leon and R. N. Zare, Factors Affecting Quantitative Analysis in Laser  
 1051 Desorption/Laser Ionization Mass Spectrometry, *Analytical Chemistry*, 2004, **76**, 2430–2437.
- 1052 72M. K. Spencer, M. R. Hammond and R. N. Zare, Laser mass spectrometric detection of  
 1053 extraterrestrial aromatic molecules: Mini-review and examination of pulsed heating effects,  
 1054 *PNAS*, 2008, **105**, 18096–18101.
- 1055 73P. M. Mayer, V. Blanchet and C. Joblin, Threshold photoelectron study of naphthalene,  
 1056 anthracene, pyrene, 1,2-dihydronaphthalene, and 9,10-dihydroanthracene, *J. Chem. Phys.*,  
 1057 2011, **134**, 244312.
- 1058 74G. Rouillé, S. Krasnokutski, D. Fulvio, C. Jäger, T. Henning, G. Garcia, X. Tang and L.  
 1059 Nahon, Dissociative photoionization of polycyclic aromatic hydrocarbon molecules carrying  
 1060 an ethynyl group, *The Astrophysical Journal*, , DOI:10.1088/0004-637X/810/2/114.
- 1061 75R. Boschi, E. Clar and W. Schmidt, Photoelectron spectra of polynuclear aromatics. III. The  
 1062 effect of nonplanarity in sterically overcrowded aromatic hydrocarbons, *J. Chem. Phys.*, 1974,  
 1063 **60**, 4406–4418.
- 1064 76M. J. S. Dewar, E. Haselbach and S. D. Worley, Calculated and observed ionization potentials  
 1065 of unsaturated polycyclic hydrocarbons; calculated heats of formation by several  
 1066 semiempirical s. c. f. m.o. methods, *Proceedings of the Royal Society of London. A.*  
 1067 *Mathematical and Physical Sciences*, 1970, **315**, 431–442.
- 1068 77M. Meot-Ner, Ion thermochemistry of low-volatility compounds in the gas phase. 3.  
 1069 Polycyclic aromatics: ionization energies, proton and hydrogen affinities. Extrapolations to  
 1070 graphite, *J. Phys. Chem.*, 1980, **84**, 2716–2723.
- 1071 78M. Kinoshita, The Absorption Spectra of the Molecular Complexes of Aromatic Compounds  
 1072 with p-Bromanil, *BCSJ*, 1962, **35**, 1609–1611.
- 1073 79E. Heilbronner, T. Hoshi, J. L. von Rosenberg and K. Hafner, Alkyl-induced, natural  
 1074 hypsochromic shifts of the 2A←2X and 2B←2X transitions of azulene and naphthalene  
 1075 radical cations, *Nouv. J. Chim.*, 1976, **1**, 105.
- 1076 80Y. Ling and C. Lifshitz, Time-Dependent Mass Spectra and Breakdown Graphs. 19.  
 1077 Fluoranthene, *J. Phys. Chem.*, 1995, **99**, 11074–11080.
- 1078 81M. A. Slifkin and A. C. Allison, Measurement of Ionization Potentials from Contact Charge  
 1079 Transfer Spectra, *Nature*, 1967, **215**, 949–950.

- 1080 82 Y. Li, L. Zhang, T. Yuan, K. Zhang, J. Yang, B. Yang, F. Qi and C. K. Law, Investigation on  
1081 fuel-rich premixed flames of monocyclic aromatic hydrocarbons: Part I. Intermediate  
1082 identification and mass spectrometric analysis, *Combustion and Flame*, 2010, **157**, 143–154.
- 1083 83 L. Klasinc, B. Kovac and H. Gusten, Photoelectron spectra of acenes. Electronic structure and  
1084 substituent effects, *Pure and Applied Chemistry*, 1983, **55**, 289–298.
- 1085 84 E. Heilbronner, R. Gleiter, H. Hopf, V. Hornung and A. De Meijere, Photoelectron-  
1086 Spectroscopic Evidence for the Orbital Sequence in Fulvene and 3, 4-Dimethylene-  
1087 cyclobutene, *Helvetica Chimica Acta*, 1971, **54**, 783–794.
- 1088 85 P. A. Clark, F. Brogli and E. Heilbronner, The  $\pi$ -Orbital Energies of the Acenes, *Helvetica*  
1089 *Chimica Acta*, 1972, **55**, 1415–1428.
- 1090 86 T. A. Cool, J. Wang, K. Nakajima, C. A. Taatjes and A. McIlroy, Photoionization cross  
1091 sections for reaction intermediates in hydrocarbon combustion, *International Journal of Mass*  
1092 *Spectrometry*, 2005, **247**, 18–27.
- 1093 87 E. E. Rennie, C. a. F. Johnson, J. E. Parker, D. M. P. Holland, D. A. Shaw and M. A. Hayes,  
1094 A photoabsorption, photodissociation and photoelectron spectroscopy study of C<sub>6</sub>H<sub>6</sub> and  
1095 C<sub>6</sub>D<sub>6</sub>, *Chemical Physics*, 1998, **229**, 107–123.
- 1096 88 S. Soorkia, A. J. Trevitt, T. M. Selby, D. L. Osborn, C. A. Taatjes, K. R. Wilson and S. R.  
1097 Leone, Reaction of the C<sub>2</sub>H Radical with 1-Butyne (C<sub>4</sub>H<sub>6</sub>): Low-Temperature Kinetics and  
1098 Isomer-Specific Product Detection, *J. Phys. Chem. A*, 2010, **114**, 3340–3354.
- 1099 89 P. Carlier and G. Mouvier, Etude par spectrometrie de photoelectrons de la structure  
1100 electronique des phenyl-alcynes conjuges, *Journal of Electron Spectroscopy and Related*  
1101 *Phenomena*, 1979, **16**, 169–181.
- 1102 90 B. West, A. Sit, A. Bodi, P. Hemberger and P. M. Mayer, Dissociative Photoionization and  
1103 Threshold Photoelectron Spectra of Polycyclic Aromatic Hydrocarbon Fragments: An  
1104 Imaging Photoelectron Photoion Coincidence (iPEPICO) Study of Four Substituted Benzene  
1105 Radical Cations, *The Journal of Physical Chemistry A*, 2014, **118**, 11226–11234.
- 1106 91 F. Zhang, R. I. Kaiser, V. V. Kislov, A. M. Mebel, A. Golan and M. Ahmed, A VUV  
1107 Photoionization Study of the Formation of the Indene Molecule and Its Isomers, *J. Phys.*  
1108 *Chem. Lett.*, 2011, **2**, 1731–1735.
- 1109 92 C. R. Brundle, M. B. Robin and N. A. Kuebler, Perfluoro effect in photoelectron  
1110 spectroscopy. II. Aromatic molecules, *J. Am. Chem. Soc.*, 1972, **94**, 1466–1475.
- 1111 93 D. Dougherty, J. Lewis, R. V. Nauman and S. P. McGlynn, Photoelectron spectroscopy of  
1112 azulenes, *Journal of Electron Spectroscopy and Related Phenomena*, 1980, **19**, 21–33.
- 1113 94 C.-H. Chin, T. Zhu and J. Z. Zhang, Theoretical Investigations of Photoionization Efficiency  
1114 of Naphthalene, , DOI:10.26434/chemrxiv.7665620.v1.
- 1115 95 R. Gleiter, W. Schäfer and M. Eckert- Maksić, Transannulare Wechselwirkungen zwischen  
1116 Acetylenen – Photoelektronenspektroskopische Untersuchungen an 1,8-Diethylnaphthalin  
1117 und cyclischen Derivaten von 2,2'-Diethylnylbiphenyl, *Chemische Berichte*, 1981, **114**, 2309–  
1118 2321.
- 1119 96 Y. Y. Li, Y. JiuZhong and C. ZhanJun, Photonization Cross Section Database (Version  
1120 2.0), <http://flame.nslr.ustc.edu.cn/database/>.
- 1121 97 J. Appel, H. Bockhorn and M. Wulkow, A detailed numerical study of the evolution of soot  
1122 particle size distributions in laminar premixed flames, *Chemosphere*, 2001, **42**, 635–645.
- 1123 98 N. A. Eaves, S. B. Dworkin and M. J. Thomson, Assessing relative contributions of PAHs to  
1124 soot mass by reversible heterogeneous nucleation and condensation, *Proceedings of the*  
1125 *Combustion Institute*, 2017, **36**, 935–945.
- 1126 99 C. A. Schuetz and M. Frenklach, Nucleation of soot: Molecular dynamics simulations of  
1127 pyrene dimerization, *Proceedings of the Combustion Institute*, 2002, **29**, 2307–2314.
- 1128 100 R. Boschi and W. Schmidt, Photoelectron spectra of polycyclic aromatic hydrocarbons.  
1129 Pyrene and coronene, *Tetrahedron Letters*, 1972, **13**, 2577–2580.

- 1130 101 K. O. Johansson, T. Dillstrom, P. Elvati, M. F. Campbell, P. E. Schrader, D. M. Popolan-  
1131 Vaida, N. K. Richards-Henderson, K. R. Wilson, A. Violi and H. A. Michelsen, Radical-  
1132 radical reactions, pyrene nucleation, and incipient soot formation in combustion, *Proceedings*  
1133 *of the Combustion Institute*, 2017, **36**, 799–806.
- 1134 102 B. D. Adamson, S. A. Skeen, M. Ahmed and N. Hansen, Detection of Aliphatically  
1135 Bridged Multi-Core Polycyclic Aromatic Hydrocarbons in Sooting Flames with Atmospheric-  
1136 Sampling High-Resolution Tandem Mass Spectrometry, *J. Phys. Chem. A*, 2018, **122**, 9338–  
1137 9349.
- 1138 103 J. W. Martin, D. Hou, A. Menon, L. Pascazio, J. Akroyd, X. You and M. Kraft,  
1139 Reactivity of Polycyclic Aromatic Hydrocarbon Soot Precursors: Implications of Localized  $\pi$ -  
1140 Radicals on Rim-Based Pentagonal Rings, *J. Phys. Chem. C*, 2019, **123**, 26673–26682.
- 1141 104 R. A. Krueger and G. Blanquart, Predicting aromatic exciplex fluorescence emission  
1142 energies, *Phys. Chem. Chem. Phys.*, 2019, **21**, 10325–10335.
- 1143
- 1144